Temporal evolution of the extreme excursions of multivariate kth order Markov processes with application to oceanographic data

Stan Tendijck[1], Philip Jonathan[1,2], David Randell[3], and Jonathan Tawn[1]

[1]Department of Mathematics and Statistics, Lancaster University LA1 4YW, United Kingdom
[2]Shell Research Limited, London SE1 7NA, United Kingdom
[3]Shell Global Solutions International B.V., 1031 HW Amsterdam, Netherlands

October 26, 2023

Abstract

We develop two models for the temporal evolution of extreme events of multivariate kth order Markov processes. The foundation of our methodology lies in the conditional extremes model of Heffernan and Tawn (2004), and it naturally extends the work of Winter and Tawn (2016, 2017) and Tendijck et al. (2019) to include multivariate random variables. We use cross-validation-type techniques to develop a model order selection procedure, and we test our models on two-dimensional meteorological-oceanographic data with directional covariates for a location in the northern North Sea. We conclude that the newly-developed models perform better than the widely used historical matching methodology for these data.

Keywords: *extreme value theory, time-series, Markov processes, oceanography*

1 Introduction

Farmers, stock brokers and sailors have one thing in common: they or their businesses are most heavily affected by extreme events like droughts and rainfall, stock market crashes, or extreme winds and waves, respectively. Understanding the statistical behaviour of such events as a whole is crucial for risk analyses. To make this more precise, if we let $(\tilde{\mathbf{X}}_i)_{i\in\mathbb{Z}}$ be a stationary d-dimensional random process of interest, then we seek to model excursions of the process in and out of a set $E \subset \mathbb{R}^d$ in time, i.e., the behaviour of

$$\{\tilde{\mathbf{X}}_i : \ i = a, \ldots, b; \ \tilde{\mathbf{X}}_i \in E; \ \tilde{\mathbf{X}}_{a-1}, \tilde{\mathbf{X}}_{b+1} \notin E\}, \tag{1}$$

where E is associated with extreme events of the random variable $\mathbf{X}$, identically distributed for any time point i; moreover, we assume that any of the d components of the multivariate time-series can be extreme. To solve this task, we assume that the multivariate random process is a realisation of a kth order Markov chain. (Note that here and throughout the article, for preciseness, the tilde symbol above $\mathbf{X}_i$ indicates that $\mathbf{X}_i$ is indexed with respect to "absolute" time i. Later in the article, it will be convenient to index *excursions* of $(\tilde{\mathbf{X}}_i)_{i\in\mathbb{Z}}$ using time t relative to the time of the peak of the excursion (at $t = 0$), which we will write as $(\mathbf{X}_t)_{t\in\mathbb{Z}}$ with the tilde suppressed.)

We use extreme value theory to characterise excursions. There is considerable attention to this area in the literature, but most of extreme value theory for stationary Markov chains dates back over 20 years. Rootzén (1988) and Perfekt (1997) develop limiting results for univariate Markov chains and multivariate Markov

chains, respectively. Smith (1992) calculates the extremal index (Leadbetter et al., 1983) for a univariate Markov chain and Smith et al. (1997) use parametric bivariate transition distributions to model the extremes of a univariate first order Markov process. Finally, Yun (2000) develops asymptotic theory for functionals of univariate kth order Markov extreme events. All of these authors derive results under the assumption of asymptotic dependence (Joe, 1997), i.e., for a stationary univariate process $(\tilde{X}_i)_{i\in\mathbb{Z}}$ satisfying suitable long-range mixing conditions, under the assumption that for any lag $l = 1, 2, \ldots$

$$\lim_{u\to x^*} \mathbb{P}(\tilde{X}_{i+l} > u | \tilde{X}_i > u) > 0,$$

where x^* is the right upper end point of the stationary distribution of X. This early work doesn't consider what happens when asymptotic independence is present, i.e., when this limiting probability converges to 0 for some l. The first paper which considers such processes is Bortot and Tawn (1998) who assume a first order Markov model, with Ledford and Tawn (2003) considering a general framework for the modelling of asymptotic independent processes, and key recent probabilistic developments given by Papastathopoulos et al. (2017) and Papastathopoulos et al. (2023).

Randell et al. (2015) speculate that a statistical model for the evolution of (multivariate) trajectories would be a valuable enhancement of description of ocean storm events. The first statistical work the current authors are aware of, that defines a model for the distribution of all observations during an excursion is Winter and Tawn (2016), who assume a flexible univariate first order Markov process exhibiting either asymptotic independence or asymptotic dependence across lags. Winter and Tawn (2017) incorporate higher order dependence models to give kth order Markov processes with $k > 1$. Finally, Tendijck et al. (2019) extend that model to a kth order univariate Markov process with a directional covariate. We remark that their work cannot be considered to model the extremes of bivariate Markov processes since the associated directional covariate does not take on extreme values. Feld et al. (2015) use a sophisticated covariate model for the most extreme observation (the most extreme value of the dominant variable) in an excursion, combined with a historical matching approach for the intra-excursion trajectory; in Section 3.4 we adopt a version of this methodology as a benchmark for our case study. Finally, we mention well-established literature on multivariate time series, e.g., Tiao and Tsay (1989), which is not directly applicable to modelling environmental extremes because such models are only designed to model typical behaviours. Financial time-series models, e.g., Bauwens et al. (2006), are also not applicable because these are specifically tailored to model data exhibiting volatility, with tail switching during extreme events (Bortot and Coles, 2003).

In this work, we present a natural extension to Tendijck et al. (2019) by defining two multivariate kth order Markov models that exhibit both asymptotic (in)dependence across variables and/or at some lags. The work is motivated by our case study in which we model excursions of meteorological-oceanographic (met-ocean) data: significant wave height, wind speed, and their associated directions, for a location in the northern North Sea. We will demonstrate the direct practical importance of a model for extremal excursions of oceanographic time-series in characterising the extreme ocean environment, and in particular the forces induced by that environment on marine structures.

We use the following set up. Assume that at each time $i \in \mathbb{Z}$, the distribution of the d-dimensional random variable $\tilde{\mathbf{X}}_i$ is stationary through time; that is, $\tilde{\mathbf{X}}_i$ has the same distribution as some $\tilde{\mathbf{X}} = (\tilde{X}_1, \tilde{X}_2, \ldots, \tilde{X}_d)$ with distribution function $F_{\tilde{\mathbf{X}}}$. For $1 \leq j \leq d$, write $F_{\tilde{X}_j}$ as the jth marginal distribution of $F_{\tilde{\mathbf{X}}}$. The distribution functions $F_{\tilde{X}_j}$ are unknown and must be estimated. For extreme arguments of $F_{\tilde{X}_j}$, we use univariate extreme value theory to motivate a class of parametric tail forms. More precisely, we assume that for each $1 \leq j \leq d$, the excesses tail above some high level $u_j \in \mathbb{R}$ of the marginal distribution $F_{\tilde{X}_j}$ are approximated with a generalised Pareto distribution (Davison and Smith, 1990). For non-extreme arguments $x < u_j$ of the function $F_{\tilde{X}_j}$, an empirical model usually suffices.

In multivariate extreme value theory, it is common to consider the marginals and the dependence of random variables separately, such that the usually-dominant marginal effect does not influence the modelling of a possibly complex dependence structure. So given the marginal models as discussed above, we transform the random process $(\tilde{\mathbf{X}}_i)_{i\in\mathbb{Z}}$ onto standard Laplace margins $(\tilde{\mathbf{Y}}_t)_{t\in\mathbb{Z}}$ using the transformation: $\tilde{X}_j \mapsto \tilde{Y}_j := F_L^{-1}(F_{\tilde{X}_j}(\tilde{X}_j))$, $1 \leq j \leq d$, where F_L^{-1} is the inverse of the standard Laplace distribution function. Here the

choice of Laplace margins is made to allow for the modelling of potential negative dependence at certain lags or across components (Keef et al., 2013).

For multivariate random processes, there are many ways of defining an extreme event. In our case study, we take the met-ocean variable significant wave height H_S as the excursion-defining component. We follow Winter and Tawn (2017) and Tendijck et al. (2019) in adopting the conditional extremes model of Heffernan and Tawn (2004), see also Section 2.2, as the foundation of our approach. Without loss of generality, we use the first component X_1 of $\mathbf{X}$ as the defining variable for the extreme events. So, we set our excursion set $E = E_u := (F_{X_1}^{-1}\{F_L(u)\}, \infty) \times \mathbb{R}^{d-1}$ for some high threshold $u \in \mathbb{R}_+$ and rewrite our definition of an excursion as

$$\{\tilde{\mathbf{Y}}_i : \ i = a, \ldots, b; \ \tilde{Y}_{i,1} > u; \tilde{Y}_{a-1,1} \leq u, \ \tilde{Y}_{b+1,1} \leq u\} \tag{2}$$

for $a, b \in \mathbb{Z}$, indices for the start and the end time points of the excursion, respectively. In shorthand, the excursion is then $\tilde{\mathbf{Y}}_{a:b}$. We remark that in this definition, we accept that multiple excursions can occur close together in time, and thus these cannot be considered independent. The reason for this choice is that imposing a minimal separation of excursions would complicate the modelling significantly. We recognize that this is a feature of the current approach which can be improved upon in future work.

Objective, novelty and outline

The objective of the current work is to develop a statistical description for the temporal evolution of excursions of multivariate time-series near a local maximum of one of the time-series components. The novelty of the new description rests in the incorporation and extension of existing methods. Specifically, the methodology presented incorporates the conditional extremes model of Heffernan and Tawn (2004), introduces a multivariate extension of the Markov extremal model of Winter and Tawn (2017), and introduces a new extremal vector autoregressive model. Following Tendijck et al. (2019), the methodology also accommodates non-stationarity of excursions with respect to covariates. From a real-world applications' perspective, we will demonstrate that the methodology developed provides better simulation of excursions compared to a baseline "historical matching" approach, in characterising extremes of structural loading from winds and waves on a notional offshore structure.

The remaining part of this paper is organised as follows. In Section 2, we present our strategy for modelling excursions by defining time intervals corresponding to so-called "pre-peak", "peak" and "post-peak" periods, and we present our kth order Markov models for each of these time periods. In Section 3, we apply the two Markov model forms we propose to met-ocean data for a location in the northern North Sea. We compare the model performance with a baseline historical matching approach by assessing their respective performance in estimating the tails of the distributions of complex structure variables (Coles and Tawn, 1994), corresponding to approximations of the response of hypothetical offshore or coastal facilities to extreme met-ocean environments. We find that in general the new models are preferred.

2 The models

2.1 Modelling strategy

To model excursions as in definition (2), two types of approaches have been proposed in the literature of univariate extremes: a forward model (Rootzén, 1988) and a peak model (Smith et al., 1997). Both of these are two-step approaches by nature. The forward model first describes the distribution of a random exceedance $\tilde{Y}_i > u$ with a univariate extremes model and a conditional model for the distribution for any $j \geq 1$ of $\tilde{Y}_{i+l}|(\tilde{Y}_{i+l-\tau} = y_{i+l-\tau}, \tau = 1, \ldots, l)$ where $y_i > u$. Even though this approach does not directly model the univariate equivalent of excursions in formulation (2), estimates of some extremal properties of the process $(\tilde{Y}_t)_{t\geq 1}$, such as the extremal index (Leadbetter et al., 1983), can still be obtained by allowing the excursion threshold to be significantly lower than the cluster threshold used in extremal index estimators. Notably, Winter and Tawn (2016, 2017) use the forward approach in their work.

The peak model, on the other hand, does model excursions as defined here. This method relies on a univariate extremes model for the largest observation of an excursion, e.g., Eastoe and Tawn (2012), and a conditional model for observations before and after the excursion maximum. Winter and Tawn (2016) use this approach for their first order model but not for their kth order model (Winter and Tawn, 2017). They avoid this method explicitly because of difficulties that arise in preserving model characteristics in forward and backward simulations near the excursion maximum (i.e., the time point at which the defining variate achieves its maximum value during the excursion; without loss of generality, we can assume that the first variate X_1 is the defining variate).

Tendijck et al. (2019) use the peak method, but they do not address the issues associated with forward and backward simulation under the method. Because the excursion maximum is usually the most important observation of an excursion for risk assessments, we also use the peak method in the current work, but with consideration of backward and forward models. We separate the modelling of excursions into three stages: the modelling of the period of the peak, and the modelling of the pre-peak and post-peak periods. Without loss of generality, let $i = i^*$ be the time point at which the first component Y_1 takes its maximum value within an excursion, and define relative time as $t = i - i^*$. Then write $(\tilde{\mathbf{Y}}_i)_{i\in[a,b]}$ as $(\mathbf{Y}_t)_{t\in[a,b]-i^*}$, such that $Y_{t=0,j=1} > u$ for threshold u is a local maximum of Y_1.

The periods of the peak $\mathcal{P}_0^k$, the pre-peak $\mathcal{P}^{\text{pre}}$ and post-peak $\mathcal{P}^{\text{post}}$ are then defined by the expressions

$$\begin{aligned}
\mathcal{P}_0^k &:= \{\mathbf{Y}_t : \ -(k-1) \le t \le k-1\} \text{ with } Y_{0,1} > u, \\
\mathcal{P}^{\text{pre}} &:= \{\mathbf{Y}_t : \ t' \le t \le 0, \text{ with } t' = \min\{s < 0 : \min_{i=s,\dots,0}\{Y_{i,1}\} > u\}\}, \\
\mathcal{P}^{\text{post}} &:= \{\mathbf{Y}_t : \ 0 \le t \le t', \text{ with } t' = \max\{s > 0 : \min_{i=0,\dots,s}\{Y_{i,1}\} > u\}\}.
\end{aligned} \tag{3}$$

Thus, for a kth order excursion, $\mathcal{P}_0^k$ consists of a set of $2k-1$ observations. The pre-peak $\mathcal{P}^{\text{pre}}$ and post-peak $\mathcal{P}^{\text{post}}$ periods are defined as the sets of observations that include the excursion maximum and the threshold exceedances before and after, respectively, so each of them intersects with $\mathcal{P}_0^k$. The length of $\mathcal{P}_0^k$ can be longer or shorter than the length of an excursion if the excursion ends within the period of the peak. We choose to define the period $\mathcal{P}_0^k$ in this manner so that the pre-peak and post-peak parts of the excursion are both initialized with k observations. Figure 1 illustrates the three time periods for the case $k = 3$.

We then model an excursion as follows: (i) we model the excursion maximum $Y_{0,1}$ using a generalised Pareto distribution; (ii) we model the period of the peak $\mathcal{P}_0^k$ conditional on the storm maximum $Y_{0,1}$ using the model described in Section 2.2; (iii-a) if $\min_{j=1,\dots,k-1} Y_{l,1} < u$ ($\min_{l=1,\dots,k-1} Y_{-l,1} < u$), then the period $\mathcal{P}^{\text{post}}$ ($\mathcal{P}^{\text{pre}}$) of the excursion has ended; (iii-b) if $\min_{l=1,\dots,k-1} Y_{l,1} \ge u$ ($\min_{l=1,\dots,k-1} Y_{-l,1} \ge u$), then the remaining part of the excursion is modelled with our time-series models from Sections 2.3-2.4 until there exist a $l_1, l_2 > 0$ such that $Y_{l_1,1} < u$ and $Y_{-l_2,1} < u$; (iv) if $\max_{-l_2\le i\le l_1} Y_{i,1} > Y_{0,1}$, then the model for the excursion contradicts the definition of the period of the peak of an excursion, and so we reject such occurrences.

Two types of forward model are introduced below, either of which can be used to describe the pre- and post-peak periods of excursions. The forward models are referred to as the multivariate Markov extremal model (MMEM), and the extremal vector autoregression (EVAR). Informally, both forward models can be viewed as extensions of the conditional extremes model of Heffernan and Tawn (2004). The canonical bivariate conditional extremes model assumes a functional form $(Y|(X = x)) = a(x) + b(x)Z$ for the relationship between random variables X and Y on standard Laplace marginal scales, for large values x, for normalising functions a, b and residual random variable Z. In this simplest setting, typical choices of $a(x)$ and $b(x)$ are αx and x^β, for parameters α and β with restricted domains. Both MMEM (discussed in Section 2.3) and EVAR (Section 2.4) describe the joint distribution of $\mathbf{Y}_{t+k}$ conditional on $(\mathbf{Y}_t, \dots, \mathbf{Y}_{t+k-1})$ when $Y_{t,1} = y > u$ for a large threshold $u > 0$, using the same functional form with suitable multivariate choices for the normalising functions, and a multivariate residual process. In addition, the period of the peak is described directly with a conditional extremes model (Section 2.2).

In the next sections, we discuss forward models that are applicable to model the post-peak period $\mathcal{P}^{\text{post}}$. We model the pre-peak period $\mathcal{P}^{\text{pre}}$ using the forward models applied to $(\mathbf{Y}_{-t})_{t\in\mathbb{Z}}$ (with potentially different parameters, although these would be the same if the process was time reversible). Importantly, we do not

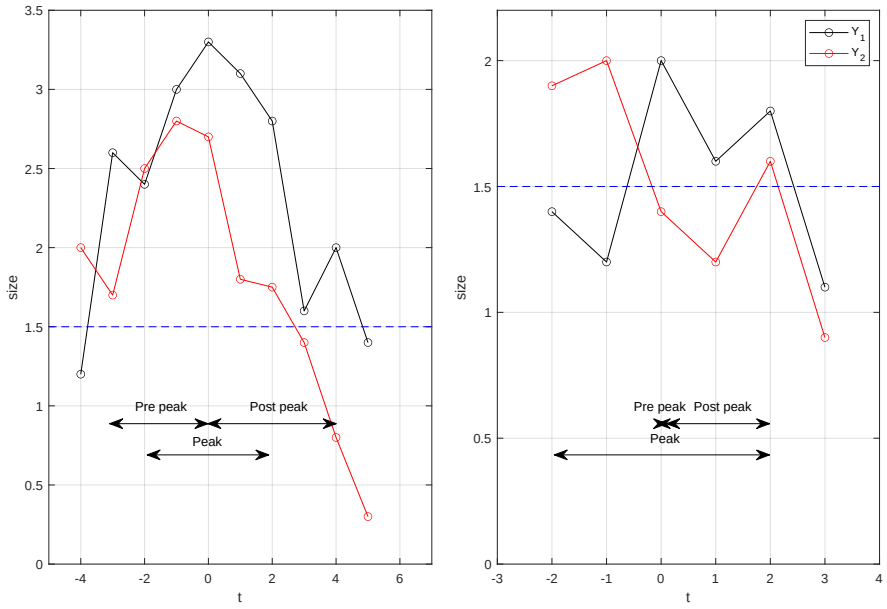

Figure 1: Illustrations of the pre-peak, peak and post-peak periods for two excursions (left and right) of a bivariate time-series with defining component Y_1 (black) and second component Y_2 (red), for a Markov model with order $k = 3$. The threshold level u is shown as a dashed blue line. Referring to Equation 3, the period of the peak $\mathcal{P}_0^k$ by definition consists of $2k - 1 = 5$ observations for the left-hand and right-hand excursions, centred on the local maximum of the defining component at $t = 0$ (despite the fact that $Y_1 < u$ for the right hand excursion at $t \leq -1$). The pre-peak period $\mathcal{P}^{\text{pre}}$ is the continuous interval, backwards in time, from the peak of Y_1 at $t = 0$ for which $Y_1 > u$. Thus, for the left- and right-hand excursions, $\mathcal{P}^{\text{pre}}$ is of length 4 and 0 respectively. The post-peak period $\mathcal{P}^{\text{post}}$ is the continuous interval, forwards in time, from the peak of Y_1 at $t = 0$ for which $Y_1 > u$. Thus, for the left- and right-hand excursions, $\mathcal{P}^{\text{post}}$ is of length 5 and 3 respectively.

impose consistency in the forward and backward models to yield a kth order Markov chain, e.g., in the case of asymptotic dependent Markov chains the precise dependence conditions between the forward and backward hidden tail chains are given by Janßen and Segers (2014). We make this choice for two reasons: (i) for environmental applications, such as in this work, the pre-peak and post-peak period have different distributions, see for example the asymmetry in Figure 5, which is due to different physics in the growth and decay of a storm; (ii) the assumption of a kth order Markov process is an approximation for the process that generates our data. Thus, imposing forward and backward consistency for a kth order Markov chain is likely to yield worse results for our application. So, we consider the violating of this assumption as a benefit more than a limitation as it can yield more flexible descriptions of excursions.

2.2 The conditional extremes model

We introduce the conditional extreme value model of Heffernan and Tawn (2004), henceforth denoted the HT model, with notation specific to modelling the period of the peak $\mathcal{P}_0^k$. The HT model is widely studied and applied to extrapolate tails of multivariate distributions, e.g., in oceanography (Ross et al., 2020), finance (Hilal et al., 2011), spatio-temporal extremes (Simpson and Wadsworth, 2021), and multivariate spatial extremes (Shooter et al., 2022). The HT model is a limit model and its form was originally motivated by deriving possible limiting forms for numerous theoretical examples.

Let

$$\mathbf{Y}_{-(k-1):(k-1)} := \begin{pmatrix} Y_{-(k-1),1} & \cdots & Y_{-(k-1),d} \\ \vdots & & \vdots \\ Y_{k-1,1} & \cdots & Y_{k-1,d} \end{pmatrix}$$

be a random matrix on $\mathbb{R}^{(2k-1)\times d}$ with standard Laplace margins (Keef et al., 2013), and define the irregular random matrix $\underline{\mathbf{Y}}$ to be $\mathbf{Y}_{-(k-1):(k-1)}$ without the $(k,1)$th element $Y_{0,1}$. That is, we define the irregular matrix $\underline{\mathbf{x}} \in \mathbb{R}^{(2k-1)d-1}$ as follows:

$$\underline{\mathbf{x}} = \begin{pmatrix} x_{-k+1,1} & x_{-k+1,2} & \cdots & x_{-k+1,d} \\ \vdots & \vdots & & \vdots \\ x_{-1,1} & x_{-1,2} & \cdots & x_{-1,d} \\ & x_{0,2} & \cdots & x_{0,d} \\ x_{1,1} & x_{1,2} & \cdots & x_{1,d} \\ \vdots & \vdots & & \vdots \\ x_{k-1,1} & x_{k-1,2} & \cdots & x_{k-1,d} \end{pmatrix},$$

such that $\underline{\mathbf{x}}$ does not contain the $(k,1)$th element. Equivalently, we can write $\underline{\mathbf{x}} = \mathbf{x}_{-(k,1)}$ for $\mathbf{x} \in \mathbb{R}^{(2k-1)\times d}$. Additionally, we assume that the joint density of $\mathbf{Y}_{-(k-1):(k-1)}$ exists.

The conditional extremes model for $\underline{\mathbf{Y}}$, conditional on $Y_{0,1}$, assumes that irregular parameter matrices $\underline{\boldsymbol{\alpha}} \in [-1,1]^{(2k-1)d-1}$, $\underline{\boldsymbol{\beta}} \in (-\infty,1)^{(2k-1)d-1}$ and a distribution function H with non-degenerate marginals on $\mathbb{R}^{(2k-1)d-1}$ (the space of irregular matrices) exist, such that for all irregular matrices $\underline{\mathbf{z}} \in \mathbb{R}^{(2k-1)d-1}$ the limit

$$\lim_{u\to\infty} \mathbb{P}\left(\frac{\underline{\mathbf{Y}} - \underline{\boldsymbol{\alpha}} Y_{0,1}}{Y_{0,1}^{\underline{\boldsymbol{\beta}}}} \leq \underline{\boldsymbol{z}},\ Y_{0,1} - u > y \;\middle|\; Y_{0,1} > u \right)$$

exists, assuming component-wise operations, and that

$$H(\underline{\mathbf{z}}) := \lim_{y\to\infty} \mathbb{P}\left(\frac{\underline{\mathbf{Y}} - \underline{\boldsymbol{\alpha}} Y_{0,1}}{Y_{0,1}^{\underline{\boldsymbol{\beta}}}} \leq \underline{\boldsymbol{z}} \;\middle|\; Y_{0,1} = y \right) \tag{4}$$

exists, where $\alpha_{i,j}$, $\beta_{i,j}$ and $z_{i,j}$ are the (i,j)th elements of $\underline{\boldsymbol{\alpha}}$, $\underline{\boldsymbol{\beta}}$ and $\underline{\mathbf{z}}$, respectively. This then implies, according to l'Hopital's rule, that for $y > 0$, $\underline{\boldsymbol{z}} \in \mathbb{R}^{(2k-1)d-1}$

$$\lim_{u\to\infty} \mathbb{P}\left(\frac{\underline{\mathbf{Y}} - \underline{\boldsymbol{\alpha}} Y_{0,1}}{Y_{0,1}^{\underline{\boldsymbol{\beta}}}} \leq \underline{\boldsymbol{z}},\ Y_{0,1} - u > y \;\middle|\; Y_{0,1} > u \right) = H(\underline{\boldsymbol{z}}) \exp(-y). \tag{5}$$

Limit (5) in turn has the interpretation that as u tends to infinity, $(\underline{\mathbf{Y}} - \underline{\boldsymbol{\alpha}} Y_{0,1}) Y_{0,1}^{-\underline{\boldsymbol{\beta}}}$ and $(Y_{0,1} - u)$ are independent conditional on $Y_{0,1} > u$, and are distributed as H and a standard exponential, respectively.

In practice, we exploit these results by assuming they hold exactly above some high finite threshold $u > 0$. So, we approximate the conditional distribution of $\underline{\mathbf{Y}} | Y_{0,1} = y$ for $y > u$, $\underline{\mathbf{y}} \in \mathbb{R}^{(2k-1)d-1}$ as

$$\mathbb{P}(\underline{\mathbf{Y}} \leq \underline{\mathbf{y}} \mid Y_{0,1} = y) = H\left(\frac{\underline{\mathbf{y}} - \underline{\boldsymbol{\alpha}} y}{y^{\underline{\boldsymbol{\beta}}}} \right), \tag{6}$$

and we assume independence of $(\underline{\mathbf{Y}} - \underline{\boldsymbol{\alpha}} Y_{0,1}) Y_{0,1}^{-\underline{\boldsymbol{\beta}}}$ and $Y_{0,1}$. There is no finite-dimensional parametric form for H, so non-parametric methods are typically applied. However, we remark that there are applications of the conditional extreme value model where the copula H is assumed to be Gaussian (Towe et al., 2019) or a Bayesian semi-parametric model is used (Lugrin et al., 2016). For inference, see Section 2.5.

2.3 Multivariate Markov extremal model

For ease of presentation, we present the multivariate Markov extremal model (MMEM) of order k only for a two-dimensional time-series $(\mathbf{Y}_t)_{t\in\mathbb{Z}}$ such that $\mathbf{Y}_t = (Y_{t,1}, Y_{t,2})$ in the notation of Section 1, i.e., $\mathbf{Y}_t$ has standard Laplace margins. We only describe a forward model that is applicable to the post-peak period $\mathcal{P}^{\text{post}}$, since the backward model has a similar construction. As mentioned in Section 2.1, we apply a different forward MMEM model to $(\mathbf{Y}_{-t})_{t\in\mathbb{Z}}$ to yield the backward model for the pre-peak period $\mathcal{P}^{\text{pre}}$. Concisely put, the MMEM exploits the HT model to estimate the distribution for $\mathbf{Y}_{t+k}$ conditional on $(\mathbf{Y}_t, \ldots, \mathbf{Y}_{t+k-1})$ when $Y_{t,1} > u$ for a large threshold $u > 0$. As in Section 2.2, for each $t \in \mathbb{Z}$, we define $\tilde{\mathbf{x}}_t \in \mathbb{R}^k \times \mathbb{R}^{k+1}$ to be an irregular matrix with $k+1$ rows and 2 columns without the element that is on the first row and first column:

$$\tilde{\boldsymbol{x}}_t = \begin{pmatrix} & x_{t,2} \\ x_{t+1,1} & x_{t+1,2} \\ \vdots & \vdots \\ x_{t+k,1} & x_{t+k,2} \end{pmatrix}.$$

Then, we assume that for a large threshold $u > 0$, there exist parameters $\tilde{\boldsymbol{\alpha}}_0 \in [-1,1]^k \times [-1,1]^{k+1}$, $\tilde{\boldsymbol{\beta}}_0 \in (-\infty, 1)^k \times (-\infty, 1)^{k+1}$, and a residual random variable $\tilde{\boldsymbol{\varepsilon}}_t$ on $\mathbb{R}^k \times \mathbb{R}^{k+1}$ with non-degenerate marginals. Similar to Winter and Tawn (2017), for $t \in \mathbb{Z}$, $l \geq 1$ when $Y_{t+l,1} > u$, we then get

$$[Y_{t+k+l,1}\ Y_{t+k+l,2}] | (\mathbf{Y}_{t+l:t+k+l-1}, Y_{t+l,1} > u) = [\alpha_{k,1},\ \alpha_{k,2}] Y_{t+l,1} + Y_{t+l,1}^{[\beta_{k,1},\ \beta_{k,2}]} \cdot \boldsymbol{\varepsilon}_{k,1:2}^{C},$$

where $\boldsymbol{\varepsilon}_{k,1:2}^{C}$ is short-hand notation for $[\boldsymbol{\varepsilon}_{k,1}, \boldsymbol{\varepsilon}_{k,2}]$ conditional on $(\boldsymbol{\varepsilon}_{1:k-1,1}, \boldsymbol{\varepsilon}_{0:k-1,2})$, and throughout component-wise operations are assumed. For inference, we refer to Section 2.5.

2.4 Extremal vector autoregression

Here, we introduce extremal vector autoregression (EVAR) for extremes of the process $(\mathbf{Y}_t)_{t\geq 1}$. This model combines the HT model with a vector autoregressive model for the joint evolution of the time-series at high levels. Here we focus on the post-peak period, but note that the pre-peak period is modelled analogously. We define an EVAR model of order k with parameters $\Phi^{(l)} \in \mathbb{R}^d \times \mathbb{R}^d$ for $l = 1, \ldots, k$ and $\mathbf{B} \in (-\infty, 1)^d$ as

$$\mathbf{Y}_{t+k} | (\mathbf{Y}_t, \ldots, \mathbf{Y}_{t+k-1}) = \sum_{l=1}^{k} \Phi^{(l)} \mathbf{Y}_{t+k-l} + y^{\mathbf{B}} \boldsymbol{\varepsilon}_t, \tag{7}$$

assuming component-wise operations, with $Y_{t,1} = y$ for $y > u$, where $u > 0$ is a large threshold and $\boldsymbol{\varepsilon}_t$ is a d-dimensional multivariate random variable that has non-degenerate margins and is independent of $(\mathbf{Y}_t, \ldots, \mathbf{Y}_{t+k-1})$. Usually for a vector autoregressive model, parameter constraints would be imposed so that the resulting process is stationary. In the current extreme value context, stationarity is not of concern to us, since we reject trajectories that exceed the excursion maximum, and stop the process once the first component dips below threshold u. We define EVAR_0 as a special case of EVAR corresponding to $\mathbf{B} = \mathbf{0}$. EVAR_0 therefore has clear similarities with a regular vector autoregressive model (Tiao and Box, 1981), yet we emphasise that there is considerable difference between the two, since the parameters of EVAR_0 do not need to yield a stationary process, and the parameters of EVAR_0 are estimated using only extreme observations. To estimate the EVAR model, we adopt the same approach as that used to estimate the HT model, see Section 2.5. As explained in Appendix A, the resulting parameter estimators $\hat{\Phi}^{(l)}$ are highly correlated. Hence a reparameterisation is introduced to reduce this correlation, and improve inference efficiency and computation.

We note that dependence between components of the response for both MMEM and EVAR models is captured by the residual processes. For a d-dimensional application, the dimension of the residual process for MMEM(k) is kd, considerably larger that the d-dimensional residual process for EVAR. For practical applications with limited sample, EVAR is in this sense more parsimonious that MMEM. In contrast, in a data-rich context, we might expect MMEM to provide more complex descriptions of dependence.

2.5 Inference for conditional models

We discuss inference for each of the conditional extremes, MMEM and EVAR models with parameter vector $\boldsymbol{\theta}$. We discuss these together because they can be summarized in the same form. Specifically, let $\mathbf{W} = (W_1, \ldots, W_d)$ be a d-dimensional random variable and assume that for some high threshold $u > 0$,

$$\mathbf{W}_{2:d} | (W_1 > u) = \mathbf{g}_1(W_1; \boldsymbol{\theta}) + \mathbf{g}_2(W_1; \boldsymbol{\theta}) \boldsymbol{\varepsilon} \tag{8}$$

for some parametric functions $\mathbf{g}_1(\,\cdot\,; \boldsymbol{\theta}) : \mathbb{R} \to \mathbb{R}^{d-1}$ and $\mathbf{g}_2(\,\cdot\,; \boldsymbol{\theta}) : \mathbb{R} \to \mathbb{R}^{d-1}_{>0}$, where

$$\mathbf{g}_1(x, \boldsymbol{\theta}) := (g_{1,2}(x, \boldsymbol{\theta}), \ldots, g_{1,d}(x, \boldsymbol{\theta})), \text{ and } \mathbf{g}_2(x, \boldsymbol{\theta}) := (g_{2,2}(x, \boldsymbol{\theta}), \ldots, g_{2,d}(x, \boldsymbol{\theta})), \text{ for } x \in \mathbb{R}$$

where $\boldsymbol{\varepsilon} = (\varepsilon_2, \ldots, \varepsilon_d)$ is a $(d-1)$-dimensional multivariate random variable that is non-degenerate in each margin and independent of W_1. As an example, for MMEM, $g_{1,j}(x) = \alpha_j x$ for some α_j and $g_{2,j}(x) = x^{\beta_j}$ for some β_j.

Next, assume that we have n observations $\mathcal{D} := \{\mathbf{w}_1, \ldots, \mathbf{w}_n\}$ of the conditional random variable $\mathbf{W} | W_1 > u$, where $\mathbf{w}_i = (w_{i1}, \ldots, w_{id})$ with $w_{i1} > u$ for $i = 1, \ldots, n$. We then infer $\boldsymbol{\theta}$ by calculating the likelihood of model (8) by temporarily assuming that the $\boldsymbol{\varepsilon}$ has a multivariate normal distribution with unknown mean $\boldsymbol{\mu} = (\mu_2, \ldots, \mu_d)$ and unknown diagonal covariance matrix $\Sigma = \boldsymbol{\sigma}^2 I$ where $\boldsymbol{\sigma}^2 = (\sigma_2^2, \ldots, \sigma_d^2)$. These assumptions imply that the mean and the variance of $\boldsymbol{\varepsilon}$ are estimated simultaneously with the model parameters. The likelihood is then evaluated as

$$L(\boldsymbol{\theta}, \boldsymbol{\mu}, \boldsymbol{\sigma}^2; \mathcal{D}) = \prod_{i=1}^{n} \prod_{j=2}^{d} \frac{1}{\sqrt{2\pi}\sigma_j g_{2,j}(w_{i1}; \boldsymbol{\theta})} \exp\left\{ -\frac{1}{2\sigma_j^2} \left(\frac{w_{ij} - g_{1,j}(w_{i1}) - \mu_j g_{2,j}(w_{i1}; \boldsymbol{\theta})}{g_{2,j}(w_{i1}; \boldsymbol{\theta})} \right)^2 \right\}.$$

Finally, the parametric assumption on the distribution of $\boldsymbol{\varepsilon}$ is discarded and estimated conditional on the parametric estimate $\hat{\boldsymbol{\theta}}$ for $\boldsymbol{\theta}$, with a kernel density $\hat{h}_{2:d}$ using the 'observations' $\{\boldsymbol{\varepsilon}_i : \ i = 1, \ldots, n\}$ where $\boldsymbol{\varepsilon}_i = (\varepsilon_{i2}, \ldots, \varepsilon_{id})$ and

$$\varepsilon_{ij} := \frac{w_{ij} - \hat{g}_{1,j}(w_{i1}; \hat{\boldsymbol{\theta}})}{\hat{g}_{2,j}(w_{i1}; \hat{\boldsymbol{\theta}})}$$

for $i = 1, \ldots, n$, $j = 2, \ldots, d$. In case of MMEM, we additionally require estimates for the density of a conditional random variable $\boldsymbol{\varepsilon}_{l+1:d|2:l} = (\varepsilon_{l+1}, \ldots, \varepsilon_d) | (\varepsilon_2, \ldots, \varepsilon_l)$ for some $l \in \{2, \ldots, d-1\}$. Given the same

set of observations, we estimate its conditional density $h_{l+1:d|2:l}$ as

$$\hat{h}_{l+1:d|2:l}(\varepsilon_{l+1},\ldots,\varepsilon_d|\varepsilon_2,\ldots,\varepsilon_l) = \frac{\hat{h}_{2:d}(\varepsilon_2,\ldots,\varepsilon_d)}{\hat{h}_{2:l}(\varepsilon_2,\ldots,\varepsilon_l)},$$

where $h_{2:l}$ is estimated as the $(l-1)$-dimensional marginal of $\hat{h}_{2:d}$.

3 Case Study - Northern North Sea

3.1 Overview

We apply MMEM, EVAR and a historical matching procedure (introduced in Section 3.4, henceforth referred to as HM) to characterise excursions of significant wave height H_S and wind speed W_s with directional covariates for a location in the northern North Sea. Our goal is to estimate parsimonious predictive models for the joint evolution of H_S and W_s time-series conditional on H_S being large.

In Section 3.2, we describe the available met-ocean data. In Section 3.3, we outline a model for the evolution of storm direction that is needed for our time-series models. Section 3.4 then summarises the HM procedure, and in Section 3.5, we introduce structure variable responses that approximate fluid drag loading on a marine structure such as a wind turbine or coastal defence. Finally, in Section 3.6, we compare the predictive performance of MMEM and EVAR (over a set of model orders) with the HM method in estimating structure variables for withheld intervals of time-series.

3.2 Data

We have 53 years of hindcast data

$$\mathcal{D} := \{(H_{S,i}, W_{s,i}, \theta_i^H, \theta_i^W) : \ i \in \mathcal{T}\}$$

indexed with finite $\mathcal{T} \subset \mathbb{Z}_{\geq 1}$ consisting of time-series for four three-hourly met-ocean summary statistics at a location in the northern North Sea (Reistad et al., 2009): significant wave height ($H_{S,i}$ in metres), wind speed ($W_{s,i}$ in metres per second), wave direction (θ_i^H in degrees) and wind direction (θ_i^W in degrees) for each $i \in \mathcal{T}$. To use MMEM and EVAR, we transform significant wave height and wind speed onto Laplace marginals: $H_{S,i}|\theta_i^H \mapsto H_{S,i}^{\mathrm{L}}$ and $W_{s,i}|\theta_i^W \mapsto W_{s,i}^{\mathrm{L}}$, e.g., using directional marginal extreme value models for the tails (Chavez-Demoulin and Davison, 2005), but ignoring seasonality. This part of the analysis has been reported on numerous occasions, see for example Randell et al. (2015). Because the marginal transformation includes direction as a covariate and because direction is not constant during an excursion, we also establish a model for the directional evolution of excursions in order to transform them between standard and original margins, see Section 3.3.

Let $\mathcal{D}^L$ be the collection of transformed data

$$\mathcal{D}^L := \{(H_{S,i}^L, W_{s,i}^L, \theta_i^H, \theta_i^W) : \ i \in \mathcal{T}\}.$$

To define excursions in $\mathcal{D}^L$, we set the excursion threshold u equal to the 95% percentile of a standard Laplace distribution, i.e., $u \approx 2.3$, yielding $1,467$ observations of extreme excursions $\mathcal{E}_u$. This choice of threshold is not unusual as similar conclusions are drawn for excursion thresholds that are slightly different from our original choice.

Figure 2 shows four intervals of the time-series chosen to contain the observations corresponding to the 100%, 95%, 90% and 85% sample percentiles of the set of excursion maximum significant wave heights, on original and standard Laplace margins, with directional covariates. Excursions are centred around extreme events. There is a large dependence of H_S and W_s on both original and standard margins. Moreover, variables associated to significant wave height, i.e., H_S, H_S^L and θ^H, are much smoother than their wind speed counterparts. Additionally, the directional covariates θ^H and θ^W centre around each other with no large deviations during extreme events.

In Figure 3, we visualize the (across variable joint) dependence of key variables H_S^L and W_s^L on Laplace scale at time lags up to lag 4 using a series of scatterplots where a unit of lag corresponds to three hours of observation time. The figure illustrates the complex dependence of the bivariate time-series of significant wave height and wind speed on Laplace margins. As expected, we observe (slow) convergence to an independent variable model as lag increases. Most notably, we observe a similar level of dependence of $(H_{S,t}^L, W_{s,i+4}^L)$ and $(W_{s,i}^L, W_{s,i+4}^L)$ which suggests counter-intuitively that $H_{S,i}^L$ would be a better predictor for $W_{s,i+4}^L$ than $W_{s,i}^L$.

In Figure 4, we plot (cross) correlation functions for these variables, and also for the change in directional covariates at various lags. These show that the dependence of $(H_{S,i}^L, H_{S,i+l}^L)$ decays relatively slowly as l grows to 90 hours, and that indeed the cross dependence between $(H_{S,i}^L, W_{s,i+l}^L)$ is larger than the dependence of $(W_{s,i}^L, W_{s,i+l}^L)$ for large l. Finally, the correlation plot of the change in directional covariates $\Delta\theta_{S,i}^H := (\theta_{S,i+1}^H - \theta_{S,i}^H, \text{ mod } 360)$ and $\Delta\theta_{s,i}^W := (\theta_{s,i+1}^W - \theta_{s,i}^W, \text{ mod } 360)$ on the right shows that a first order model for these covariates is appropriate since the correlations nearly vanish at lag 2 (for wind and wave) or 6 hours (for all other combinations).

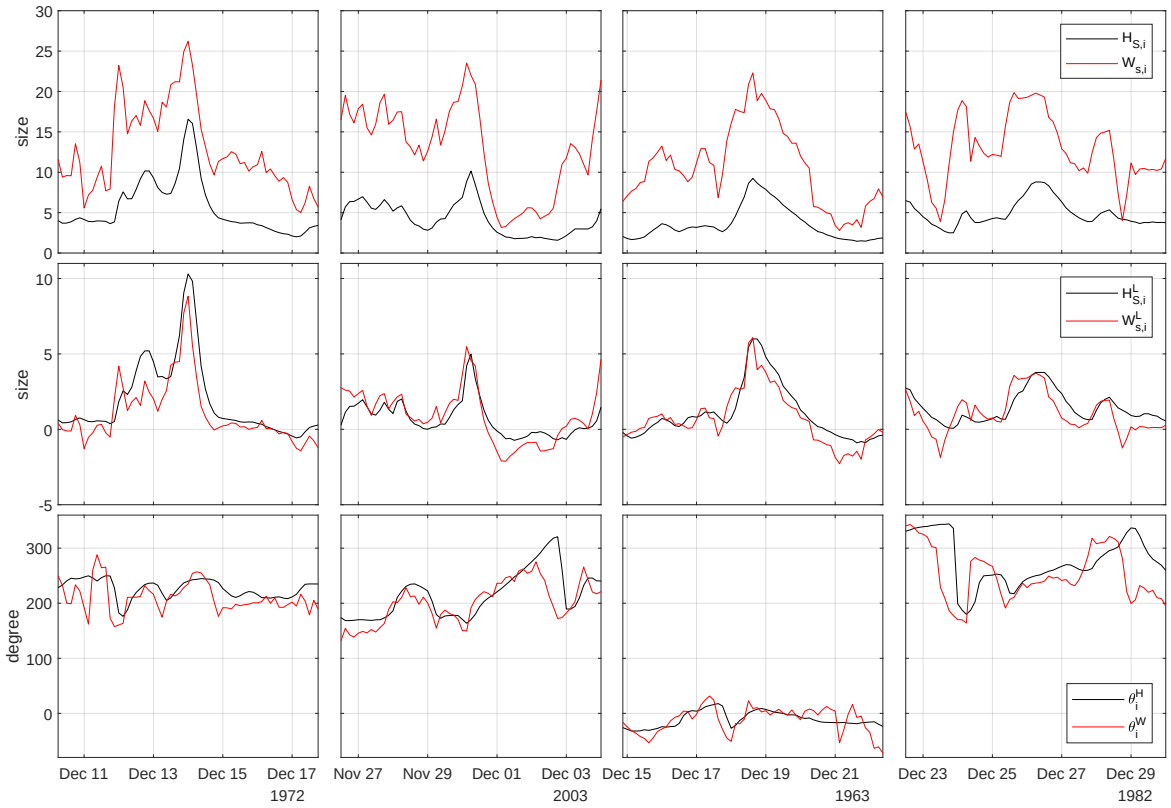

Figure 2: Intervals of oceanographic time-series: (top) key variables: significant wave height $H_{S,i}$ and wind speed $W_{s,i}$ on original margins; (middle) on Laplace margins; (bottom) covariates: wave direction θ_i^H and wind direction θ_i^W. The four columns correspond to time periods that contain the 100%, 95%, 90% and 85% empirical percentiles of $H_{S,i}$, respectively.

3.3 Directional model

We model wave direction θ_i^H in a similar fashion as Tendijck et al. (2019), summarised as follows. Let $\mathcal{I} \subset \mathcal{T}$ be the set of indices of the original data that correspond to all observations of any excursion.

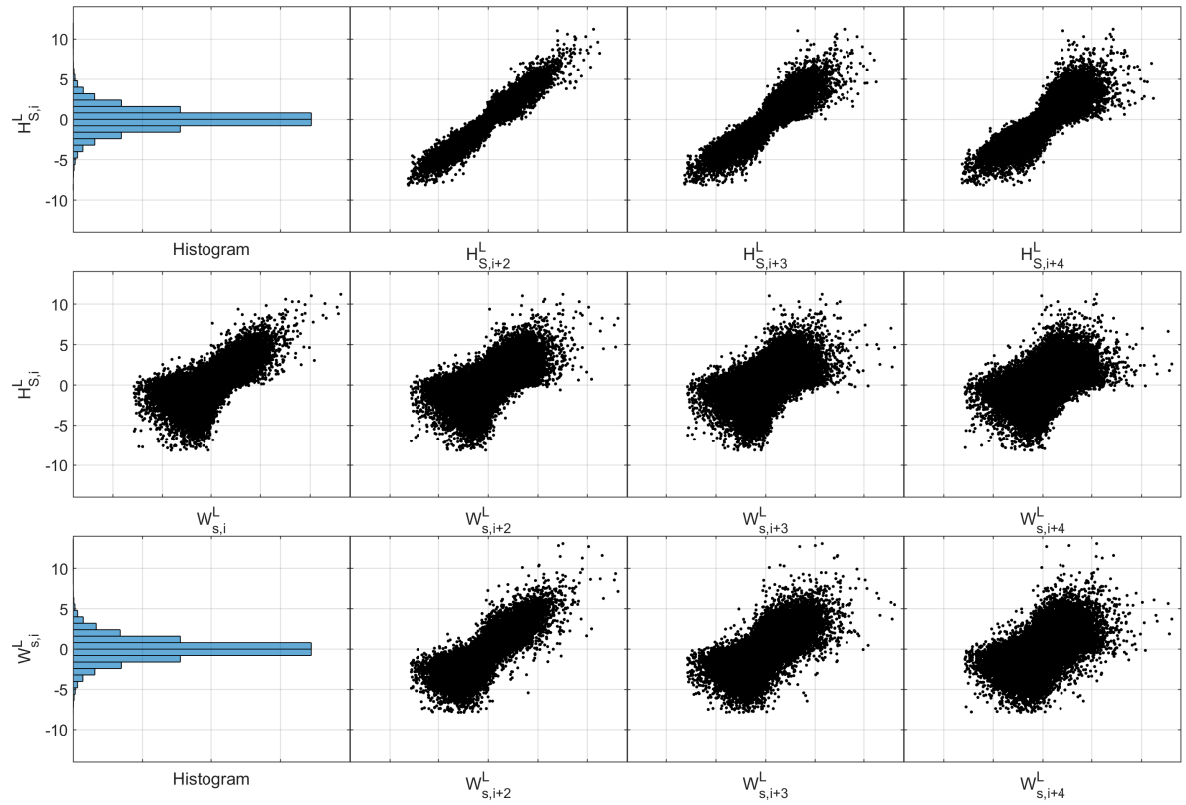

Figure 3: Matrix plot of observed $H^{\mathrm{L}}_{S,i}$ and $W^{\mathrm{L}}_{s,i}$ at various time lags up to lag 4 (corresponding to 12 hours in real time) including cross dependece.

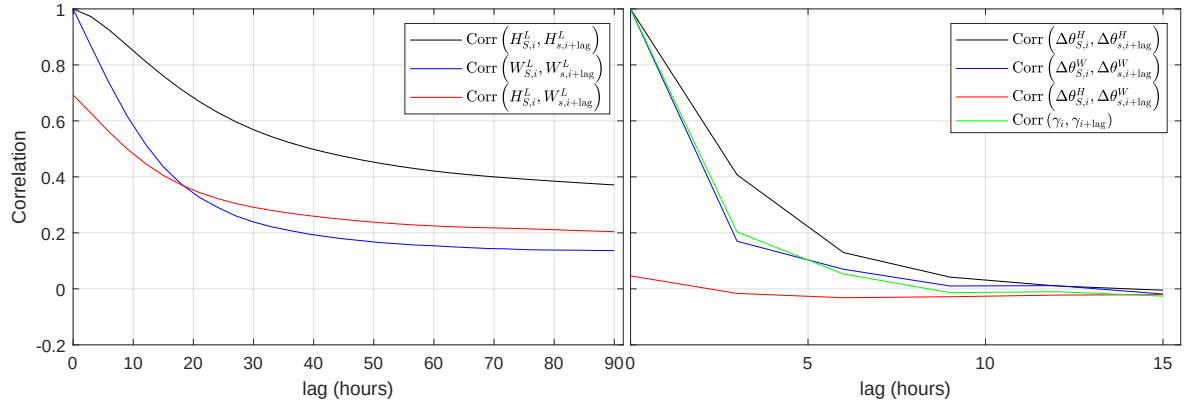

Figure 4: Estimated correlation and cross-correlation at various time lags of: (left) the key variables on Laplace margins: $H^L_{S,i}$ and $W^L_{s,i}$; (right) the covariates: change in wave direction $\Delta\theta^H_i := (\theta^H_{i+1} - \theta^H_i, \mod 360)$, change in wind direction $\Delta\theta^W_i := (\theta^W_{i+1} - \theta^W_i, \mod 360)$ and γ_i, see definition (10).

Next, let $\{d(\theta^H_{i+1}, \theta^H_i) : \ i \in \mathcal{I}\}$ be the set of changes in wave directions, where $d(\theta, \theta') = (\theta - \theta' + 180; \mod 360) - 180 \in [-180, 180)$ denotes the circular difference of θ and θ' in degrees. In our application, the set of changes in wave directions during excursions do not contain values close to -180 or 180. In particular, all of the observed changes centre around 0.

For $i \in \mathcal{I}$, we transform observations $d(\theta^H_{i+1}, \theta^H_i) \mapsto \delta^H_i := \Phi^{-1}(\hat{F}(d(\theta^H_{i+1}, \theta^H_i)))$ on Gaussian margins, where $\hat{F}$ denotes the empirical distribution function of the set of changes in wave directions. We estimate the following autoregressive model for Δ^H_i of order $p_1 = 1, 2, 3, \ldots$ with parameters $\varphi^{\mathrm{H}}_l \in \mathbb{R}$ for $l = 1, \ldots, p_1$ as

$$\Delta^H_i | (\Delta^H_{i-1}, \ldots, \Delta^H_{i-p_1}) = \sum_{l=1}^{p_1} \varphi^{\mathrm{H}}_l \Delta^H_{i-l} + \zeta(H_{S,i})\varepsilon_i, \tag{9}$$

where ε_i is a standard Gaussian random variable, and standard error $\zeta(h)$ is given by

$$\zeta^2(h) = \lambda_1 + \lambda_2 \exp(-\lambda_3 h)$$

with $\lambda_{l'} > 0$ for $l' = 1, 2, 3$, see Tendijck et al. (2019). In particular, the standard error $\zeta(h)$ decays as h grows due to the significantly larger amounts of energy needed to change the direction of more severe sea states. The parameters of this model are inferred with maximum likelihood, and in contrast to the inference discussed in Section 2.5, we do not reject the assumption that ε_i is a standard Gaussian. In practice, we use $p_1 = 1$ in line with Tendijck et al. (2019).

Given model (9), we propose the following model

$$\theta^W_i = \theta^H_i + \gamma_i \mod 360 \tag{10}$$

for wind direction θ^W_i conditional on wave direction θ^H_i, where γ_i is a zero-mean stationary AR(p_2) process. That is, there exist parameters $\varphi^{\mathrm{W}}_l \in \mathbb{R}$, $1 \leq l \leq p_2$, and a non-degenerate residual distribution r_i independent of γ_{i-l}, such that

$$\gamma_i | (\gamma_{i-1}, \ldots, \gamma_{i-p_2}) = \sum_{l=1}^{p_2} \varphi^{\mathrm{W}}_l \gamma_{i-l} + r_i,$$

and such that the polynomial $1 - \sum_{l=1}^{p_2} \varphi^{\mathrm{W}}_l z^l$ has roots outside the unit circle. The model parameters and the distribution of r_i are inferred as described in Section 2.5 conditional on the model order p_2, which is selected by investigating the correlation function in Figure 4 and the partial autocorrelation function of γ_i (not reported). In our application, we conclude that $p_2 = 1$ is sufficient.

3.4 Historical matching

An empirical method for simulating excursions is described in Feld et al. (2015) and termed historical matching (HM) in this work. They model trajectories of significant wave height, wave direction, season and wave period during extreme events. The key assumption they make is that storm trajectory (or excursion) profiles are not independent of storm maximum conditions. Specifically, the HM approach is a composition of four models: (i) a model for storm maximum wave direction; (ii) a model for storm maximum significant wave height conditional on storm maximum wave direction; (iii) a model that selects at random a historical storm trajectory with similar storm maximum characteristics to that simulated; (iv) a model that adjusts the historical storm trajectory by matching storm maximum characteristics of simulated and historical storms.

Specific details of the individual models are as follows, but this level of detail is not required for understanding the impact of the core methodology developments in Section 3. For model (i), we simply sample at random from the observed wave directions associated with storm maximum significant wave height (excursion maximum). In model (ii), storm maximum significant wave height are modelled using a generalised Pareto distribution conditional on the sampled storm maximum wave direction using a generalised additive model with the parameters as B-splines conditional on directional covariates (Chavez-Demoulin and Davison, 2005). In model (iii), we use a distance measure to calculate the dissimilarity between pairs of storm maximum

significant wave heights and storm maximum wave directions for simulated and historical trajectories. Here, we use the heuristic recommended by Feld et al. (2015) ensuring that a difference of 5 degrees in storm maximum wave direction corresponds to the same dissimilarity as $0.5m$ of difference in storm maximum significant wave height; one of the closest 20 matching storms is then selected at random for associated with the simulated storm maximum. In model (iv), we match the variables of the chosen historical trajectory as follows: (a) the historical significant wave height series are multiplied by the ratio of the simulated maximum significant wave height to the maximum of the historical significant wave height; (b) the historical wave directions are shifted such that the storm maximum wave directions of simulated and historical trajectories coincide; (c) the associated historical wind directions are rotated in the exact same way as wave direction; (d) for the full set of historical storm maxima, storm maximum associated wind speed W_s^M (namely the value of wind speed at the time point corresponding to the storm maximum event) conditional on storm maximum significant wave height H_S^M is described using linear regression with parameters $\beta_0, \beta_1 \in \mathbb{R}$, $\sigma > 0$:

$$W_s^M | H_S^M = \beta_0 + \beta_1 H_S^M + \sigma\varepsilon$$

with ε a standard normal random variable; (e) wind speed for the selected historical trajectory is scaled linearly such that it agrees with the storm maximum associated wind speed from (d).

The main deficiencies of the HM approach are (i) it does not provide a means for modelling the extremal temporal dependence characteristics of excursions, and the extremal dependence between different components of the time-series for excursions to levels beyond those observed in the historical sample, and (ii) it does not provide a model framework for the assessment of fit or uncertainty propagation.

3.5 Response variable

The motivating underlying engineering problem is the assessment of the structural reliability of an offshore structure such as a wind turbine subject to the joint action of ocean waves and winds. In the current application, the structure variable of interest is therefore the structural load (or force) on the offshore structure due to the environment, which depends on the characteristics of temporally-varying wave and wind fields present. Specifically, we seek to understand the characteristics of extreme structural loads.

To measure the practical impact of extreme met-ocean excursions, we define structure response variables for a simple hypothetical marine offshore facility. A structure response variable is a function of the met-ocean variables, key to assessing the integrity of the design of a physical structure of interest. Specifically, we consider a structure in the form of a unit cube standing above the water, supported by thin rigid legs, with vertical cube faces aligned with cardinal directions. Only wave and wind impact on the cube itself is of interest to us, and we neglect the effects of other oceanic phenomena such as swell, surge, tide, and potential climate non-stationarity. For simplicity, we also assume that when $H_S < h$, for some known value $h > 0$, the wave impact on the structure is negligible, and structural response is dominated by wind. When $H_S \geq h$, we assume that wave impact increases cubically with H_S and quadratically with W_s (see Morison et al. 1950 and Ma and Swan 2020 for supporting literature). Hence, the impact of an extreme excursion on the structure is defined by the instantaneous response variable R

$$R(H_S, W_s, \theta^H, \theta^W; c, h) = \begin{cases} c \cdot I_W^2(W_s, \theta^H - \theta^W) & \text{for } H_S < h, \\ c \cdot I_W^2(W_s, \theta^H - \theta^W) + A(\theta^H) \cdot (H_S - h) \cdot H_S^2 & \text{for } H_S \geq h, \end{cases}$$

where $I_W : \mathbb{R}_{>0} \times [-180, 180) \to \mathbb{R}$ is the inline wind-speed, defined below, $A : [-180, 180) \to [1, \sqrt{2}]$ is the exposed cross-sectional area of the cube, see below, and the parameter $c > 0$ is specified such that both significant wave height and wind speed have an approximately equal contribution to the largest values of R. Here both c and h are values that can be changed by altering structural features. The exposed cross-sectional area $A(\theta) \in [1, \sqrt{2}]$ of the cube is given by

$$A(\theta^H) := 1/\cos([(\theta^H + 45;\ \text{mod} 90) - 45] \cdot \pi/180)$$

for a given wave direction θ^H. The inline wind-speed I_W is the component of the wind speed in the direction of the wave given by

$$I_W(W_s, \theta^H - \theta^W) = W_s \cos((\theta^H - \theta^W) \cdot \pi/180).$$

To simplify notation, we write $R_i(c,h) := R(H_{S,i}, W_{s,i}, \theta_i^H, \theta_i^W; c, h)$ for $i \in \mathcal{T}$. To define a structure response for a complete excursion $\mathcal{E}_u$, we write

$$\mathcal{E}_u := \{(H_{S,i}, W_{s,i}, \Theta_i^H, \Theta_i^W) : \ a \leq i \leq b\},$$

for some $a < b$ such that for a threshold $u > 0$ (on Laplace margins) $H_{S,i}^L > u$ for $a \leq i \leq b$ and $H_{S,a-1}^L, H_{S,b+1}^L \leq u$. Next, let $i^* := i^*(\mathcal{E}_u)$ be the time of the excursion maximum, i.e., H_{S,i^*} is the maximum of $H_{S,i}$ over $\mathcal{E}_u$. We define two natural structure response variables representing the maximum impact of an excursion $\max_{\{a \leq i \leq b\}} R_i(c,h)$, and the cumulative impact of an excursion $\sum_{\{a \leq i \leq b\}} R_i(c,h)$, respectively. For our application, we consider slight alterations $R^{\max}(c,h,\mathcal{E}_u)$ and $R^{\text{sum}}(c,h,\mathcal{E}_u)$

$$R^{\max}(c,h,\mathcal{E}_u) := \max_{\{a \leq i \leq b, \ |i-i^*|>2\}} R_i(c,h), \qquad R^{\text{sum}}(c,h,\mathcal{E}_u) := \sum_{\{a \leq i \leq b, \ |i-i^*|>2\}} R_i(c,h).$$

That is, we consider responses that do not depend directly on the characteristics of the excursion near to the excursion maximum, to exaggerate the dependence of the structure variables on pre-peak and post-peak periods compared to the period of the peak, and hence the importance of estimating good models for the pre-peak and post-peak periods using MMEM or EVAR. Moreover, we define $R^{\max}(c,h)$ and $R^{\text{sum}}(c,h)$ as the random structure responses related to a random excursion.

3.6 Model comparisons

Here, we use our time-series models to characterise extreme excursions for the met-ocean data $\mathcal{D}$ of Section 3.2 with structure responses $R^{\max}$ and R^{sum}. First, we investigate the model fits, then we describe our model comparison procedure, and finally we assess model performance using a visual diagnostic.

We fit a total of EVAR, EVAR$_0$ and MMEM models with model orders $k = 1, 2, \ldots, 6$ to data $\mathcal{D}^L$, corresponding to a total of $3 \times 6 = 18$ inferences. Estimation of MMEM and EVAR models of order k for the pre- and post-peak periods requires a starting interval of k points from the peak of the defining time-series component at $t = 0$. These are provided by the HT model for the period of the peak, which must be consequently of order at least k. In this work, we therefore assume that the same model order is used to describe all of the periods $\mathcal{P}_0^k$, $\mathcal{P}^{\text{pre}}$ and $\mathcal{P}^{\text{post}}$. The choice of optimal model order for MMEM and EVAR is based on an assessment of the performance of models of different orders in reproducing the characteristics of extreme structural responses from Section 3.5 reported in Figure 7, discussed later in this section. Note that, in referring to a model briefly as 'MMEM(4)' for example, we are actually referring to a model which adopts an MMEM model of order 4 for the pre- and post-peak periods, together with a HT model of order 4 for the period of the peak.

The fitting of these 18 models is a two-stage procedure. In the first part, we fit (six) conditional extremes models for the period of the peak $\mathcal{P}_0^k$ for each k. Given the conditional extremes model for some order for the period of the peak, we are then able to estimates each of $2 \times 18 = 36$ models of the same order for the pre-peak $\mathcal{P}^{\text{pre}}$ and post-peak $\mathcal{P}^{\text{post}}$ periods. We find that a model order $k = 4$ for both MMEM and EVAR is optimal in reproducing the characteristics of extreme structural responses from Section 3.5 reported in Figure 7, discussed later in this section. In Table 1, we report parameter estimates for the HT model of the period of the peak. Tables 2-3 then give parameter estimates on $\mathcal{P}^{\text{post}}$ and $\mathcal{P}^{\text{pre}}$ for MMEM(4); Table 4 reports analogous estimates for EVA(4) on post- and pre-peak periods.

The presentation of parameter estimates and their uncertainties for HT(4) and MMEM(4) in Tables 1-3 follows the model specifications in Section 2.2 and 2.3. The corresponding tables indicate that HT and MMEM models agree on some level of asymptotic independence at each lag for both pre- and post-peak periods, since coefficients of both $\underline{\boldsymbol{\alpha}}$ and $\tilde{\boldsymbol{\alpha}}_0$ are less than unity in Tables 1-3. The MMEM models also

$\underline{\boldsymbol{\alpha}}$		$\underline{\boldsymbol{\beta}}$	
0.54 (0.53,0.55)	0.58 (0.56,0.59)	0.68 (0.59,0.72)	0.36 (0.31,0.52)
0.67 (0.66,0.68)	0.75 (0.73,0.76)	0.76 (0.66,0.82)	0.34 (0.32,0.41)
0.86 (0.85,0.87)	0.91 (0.90,0.93)	0.82 (0.61,1.00)	0.08 (0.07,0.14)
	0.86 (0.84,0.87)		0.27 (0.20,0.29)
0.88 (0.87,0.88)	0.61 (0.59,0.62)	0.75 (0.52,0.96)	0.46 (0.33,0.47)
0.73 (0.72,0.74)	0.46 (0.45,0.47)	0.64 (0.62,0.80)	0.46 (0.35,0.56)
0.61 (0.60,0.62)	0.36 (0.34,0.37)	0.49 (0.48,0.66)	0.16 (-0.03,0.35)

Table 1: Estimates of the HT model parameters $\underline{\boldsymbol{\alpha}}$ and $\underline{\boldsymbol{\beta}}$ for the period of the peak $\mathcal{P}_0^k$ with model order $k = 4$. Also shown in parentheses are 90% bootstrap confidence intervals. The structure of the irregular matrix estimates of $\underline{\boldsymbol{\alpha}}$ and $\underline{\boldsymbol{\beta}}$ is explained in Section 2.2.

$\tilde{\boldsymbol{\alpha}}_0$		$\tilde{\boldsymbol{\beta}}_0$	
	0.74 (0.73, 0.75)		0.37 (0.29, 0.38)
0.86 (0.86, 0.87)	0.56 (0.55, 0.57)	0.36 (0.35, 0.44)	0.36 (0.26, 0.46)
0.73 (0.72, 0.74)	0.44 (0.43, 0.45)	0.46 (0.45, 0.51)	0.31 (0.20, 0.39)
0.63 (0.62, 0.64)	0.35 (0.34, 0.37)	0.44 (0.43, 0.54)	0.13 (0.01, 0.22)
0.55 (0.54, 0.56)	0.29 (0.27, 0.31)	0.29 (0.28, 0.51)	0.05 (-0.06, 0.16)

Table 2: Estimates of MMEM model parameters $\tilde{\boldsymbol{\alpha}}_0$ and $\tilde{\boldsymbol{\beta}}_0$ with model order $k = 4$ for $\mathcal{P}^{\text{post}}$. Also shown in parentheses are 90% bootstrap confidence intervals. The structure of the irregular matrix estimates of $\tilde{\boldsymbol{\alpha}}$ and $\tilde{\boldsymbol{\beta}}$ is explained in Section 2.3.

$\tilde{\boldsymbol{\alpha}}_0$		$\tilde{\boldsymbol{\beta}}_0$	
	0.93 (0.92, 0.95)		0.06 (0.05, 0.09)
0.84 (0.83, 0.84)	0.88 (0.87, 0.90)	0.29 (0.28, 0.49)	0.10 (0.09, 0.16)
0.67 (0.67, 0.69)	0.73 (0.72, 0.74)	0.46 (0.45, 0.55)	0.25 (0.24, 0.36)
0.56 (0.55, 0.57)	0.60 (0.59, 0.61)	0.52 (0.51, 0.59)	0.32 (0.31, 0.45)
0.48 (0.47, 0.50)	0.50 (0.49, 0.52)	0.42 (0.41, 0.56)	0.37 (0.27, 0.44)

Table 3: Estimates of MMEM model parameters $\tilde{\boldsymbol{\alpha}}_0$ and $\tilde{\boldsymbol{\beta}}_0$ with model order $k = 4$ for $\mathcal{P}^{\text{pre}}$. Also shown in parentheses are 90% bootstrap confidence intervals. The structure of the irregular matrix estimates of $\tilde{\boldsymbol{\alpha}}$ and $\tilde{\boldsymbol{\beta}}$ is explained in Section 2.3.

show decreasing levels of dependence as lag increases, indicated by decreasing values of coefficients of $\tilde{\boldsymbol{a}}_0$ for entries lower in Tables 2 and 3.

The presentation of parameter estimates and their uncertainties for EVAR(4) in Table 4 follows the model specification in Section 2.4. For each of pre- and post-peak periods, estimates for each of the 2×2 matrices $\Phi^{(l)}$, $l = 1, 2, 3, 4$ are given. Then, for example, the elements (1,1), (1,2), (2,1) and (2,2) of $\Phi^{(l=1)}$ for the post-peak period give parameter coefficients for $H^L_{S,t+4}$ on $H^L_{S,t+3}$, $H^L_{S,t+4}$ on $W^L_{s,t+3}$, $W^L_{s,t+4}$ on $H^L_{S,t+3}$ and $W^L_{s,t+4}$ on $W^L_{s,t+3}$ respectively, and their 90% bootstrap confidence bands. Results for EVAR(4) also reflect physical intuition regarding wind-driven waves in the current application. For example, the value 0.73 of $\Phi^{(1)}(2,1)$ for $\mathcal{P}^{\text{pre}}$ indicates stronger coupling on Laplace scale between W_s at lag 4 (into the past) on H_S a lag 3 (into the past) than the coupling $\Phi^{(1)}(2,2)$ between W_s and itself at the same lags. This is consistent with winds creating waves, also suggested by Figure 4. A number of parameter estimates in matrices $\Phi^{(3)}$ and $\Phi^{(4)}$ for $\mathcal{P}^{\text{post}}$ and $\mathcal{P}^{\text{pre}}$ are near zero, but there are significant elements in each matrix except for $\Phi^{(4)}$ pre-peak.

Post-peak			Pre-peak		
$\Phi^{(1)}$	1.32 (1.28, 1.36)	0.13 (0.11, 0.15)	$\Phi^{(1)}$	1.34 (1.30, 1.38)	-0.15 (-0.18, -0.12)
	0.43 (0.33, 0.52)	0.82 (0.76, 0.88)		0.73 (0.66, 0.80)	0.58 (0.51, 0.65)
$\Phi^{(2)}$	-0.42 (-0.47, -0.36)	-0.09 (-0.12, -0.07)	$\Phi^{(2)}$	-0.40 (-0.45, -0.34)	0.05 (0.03, 0.08)
	-0.27 (-0.39, -0.16)	-0.08 (-0.13, -0.02)		-0.43 (-0.55, -0.32)	0.04 (-0.02, 0.09)
$\Phi^{(3)}$	0.00 (-0.04, 0.05)	-0.04 (-0.06, -0.02)	$\Phi^{(3)}$	0.01 (-0.03, 0.06)	-0.00 (-0.02, 0.01)
	-0.02 (-0.12, 0.08)	-0.08 (-0.12, -0.04)		0.09 (-0.02, 0.19)	-0.05 (-0.09, -0.01)
$\Phi^{(4)}$	0.00 (-0.02, 0.02)	0.01 (-0.01, 0.02)	$\Phi^{(4)}$	-0.01 (-0.04, 0.01)	0.01 (-0.01, 0.02)
	-0.02 (-0.08, 0.03)	0.04 (0.01, 0.07)		-0.04 (-0.09, 0.04)	0.01 (-0.03, 0.04)
$\mathbf{B}$	0.18 (0.01, 0.32)	-0.22 (-0.41, -0.01)	$\mathbf{B}$	0.36 (0.17, 0.43)	0.15 (-0.03, 0.34)

Table 4: Estimates of EVAR model parameters (Section 2.4) with model order $k = 4$ for $\mathcal{P}^{\text{post}}$ and $\mathcal{P}^{\text{pre}}$. Also shown in parentheses are 90% bootstrap confidence intervals.

For each of the 18 models and HM, we simulate 20,000 excursions to estimate model properties. First, we illustrate model characteristics for EVAR(4) in Figure 5 by plotting simulated excursions such that the excursion maximum significant wave height takes on values between 11.5m and 12.5m (left). We visually compare these with observed excursions for the same interval of excursion maxima (middle). On the right, we summarize simulated and observed excursions in terms of the median, the 10% and 90% percentiles of the sampling distribution at each time period. Finally, in the bottom panel we plot

$$\mathbb{P}\left(\min\{H^L_{S,i} : \ i = \min(0,\tau), \ldots, \max(0,\tau)\} > u \;\middle|\; H_{S,0} \in [11.5, 12.5]\right), \tag{11}$$

for $\tau \in \mathbb{Z}$, i.e., we plot the survival probability for an excursion relative to the time of the excursion maximum, conditional on the excursion maximum taking a value between 11.5m and 12.5m for both the simulated excursions and the observed excursions. We observe good agreement in the distribution of the length of an excursion with respect to the excursion maximum as both estimates are close to each other.

In the supplementary material, we produce analogous plots for each of the 18 models considered and HM. We observe that EVAR(4) characterizes the period of the peak, and also the pre-peak and post-peak periods of the excursion well. Moreover, EVAR(4) also reproduces the observed excursion survival probability.

Next, in Figure 6, we plot estimates of conditional probabilities $\chi_H(u,l) := \mathbb{P}(H^L_{S,i+l} > u \mid H^L_{S,i} > u)$, $\chi_{HW}(u,l) := \mathbb{P}(W^L_{s,i+l} > u \mid H^L_{S,i} > u)$, and $\chi_W(u,l) := \mathbb{P}(W^L_{S,i+l} > u \mid W^L_{S,i} > u)$ using EVAR, MMEM and HM with model orders 1 and 4, and we compare these with empirical estimates.[1] We make the following observations: HM is significantly worse at characterizing each of χ_H, χ_W and χ_{HW} compared to EVAR and MMEM. Moreover, estimates obtained from EVAR of large enough order, e.g., $k \geq 4$, agree well with

[1]We leave out EVAR_0 in this analysis for conciseness since its estimates are very similar to the estimates obtained using EVAR of the same model order.

empirical estimates. MMEM, on the other hand, yields estimators that are slightly positively biased. In particular, larger model orders yield considerable improvements.

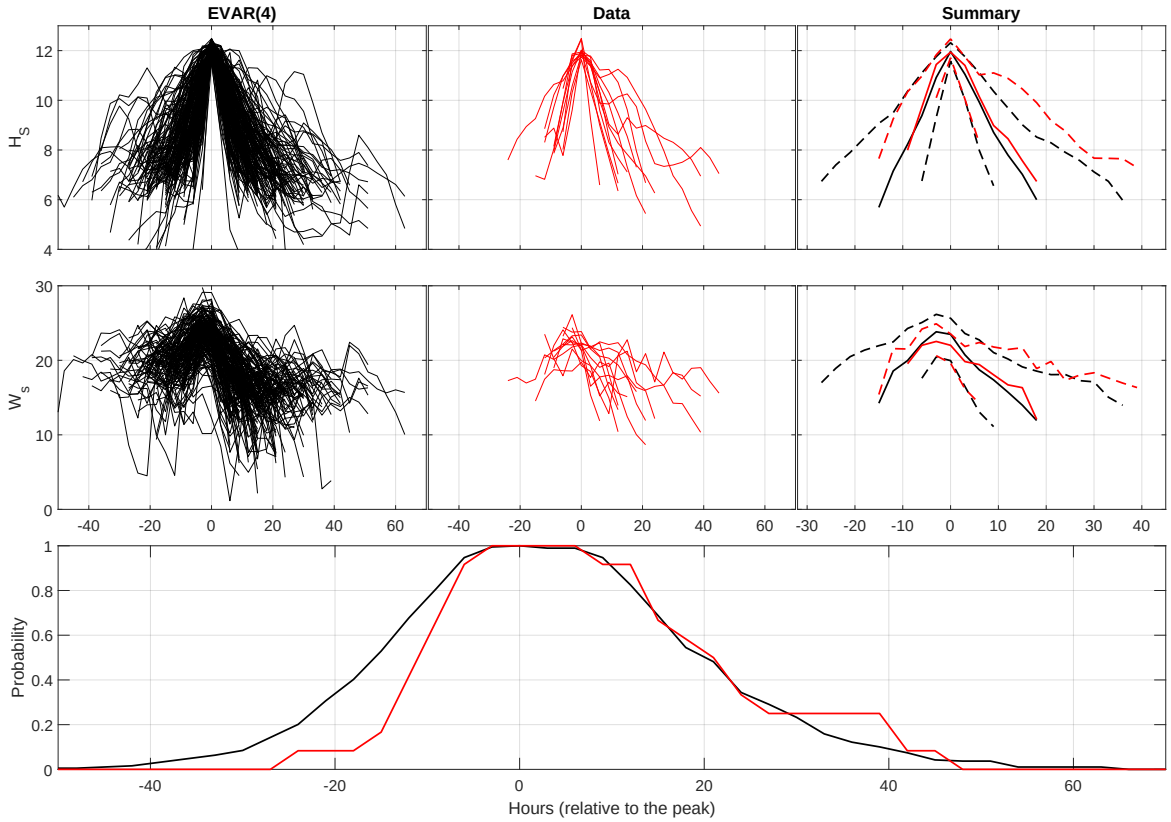

Figure 5: Excursions of H_S (top row) and W_s (middle row) from EVAR(4) model (left; black), and observed data (middle; red) on original margins such that storm peak significant wave height is in $[11.5, 12.5]$; right-hand plots summarise the observed (red) and EVAR(4) (black) excursions, in terms of the median (solid), and the 10% and 90% quantiles (dashed). In the bottom panel, we plot survival probabilities for observed (red) and EVAR(4) (black) excursions relative to the time of the excursion maximum, see equation (11).

In Figure 6, we discuss goodness-of-fit of each of the models. To compare MMEM and EVAR with each other and with HM, we take a similar approach to Gandy et al. (2022), who adjust standard cross-validation techniques to extreme value applications by taking a small training set and a larger test set. We select at random 25% of the observed excursions for our training sample; the remaining 75% forms our test sample. Below, we calculate performance statistics for the response variables by averaging over 50 such random partitions of the sample.

For training, we fit EVAR, EVAR_0 and MMEM with model orders $k = 1, 2, \ldots, 6$ as explained in the second paragraph of this section. For each of the 18 models and HM, we simulate $20,000$ excursions, calculate structure response variables $R^{\max}$ and R^{sum}, and compare distributions of simulated structure response variables with those corresponding to the withheld test data. This is achieved by defining a dissimilarity distance function D that measures the level of difference in tails of distribution functions. We select 20 equidistant percentiles $p_1, \ldots, p_{20}$ ranging from 97% to 99.9% corresponding to moderately extreme to very extreme levels with respect to the (smaller) training sample but not too extreme for the (larger) withheld data. We define the distance D of distribution functions F_M (of model M) and F_E (an empirical distribution

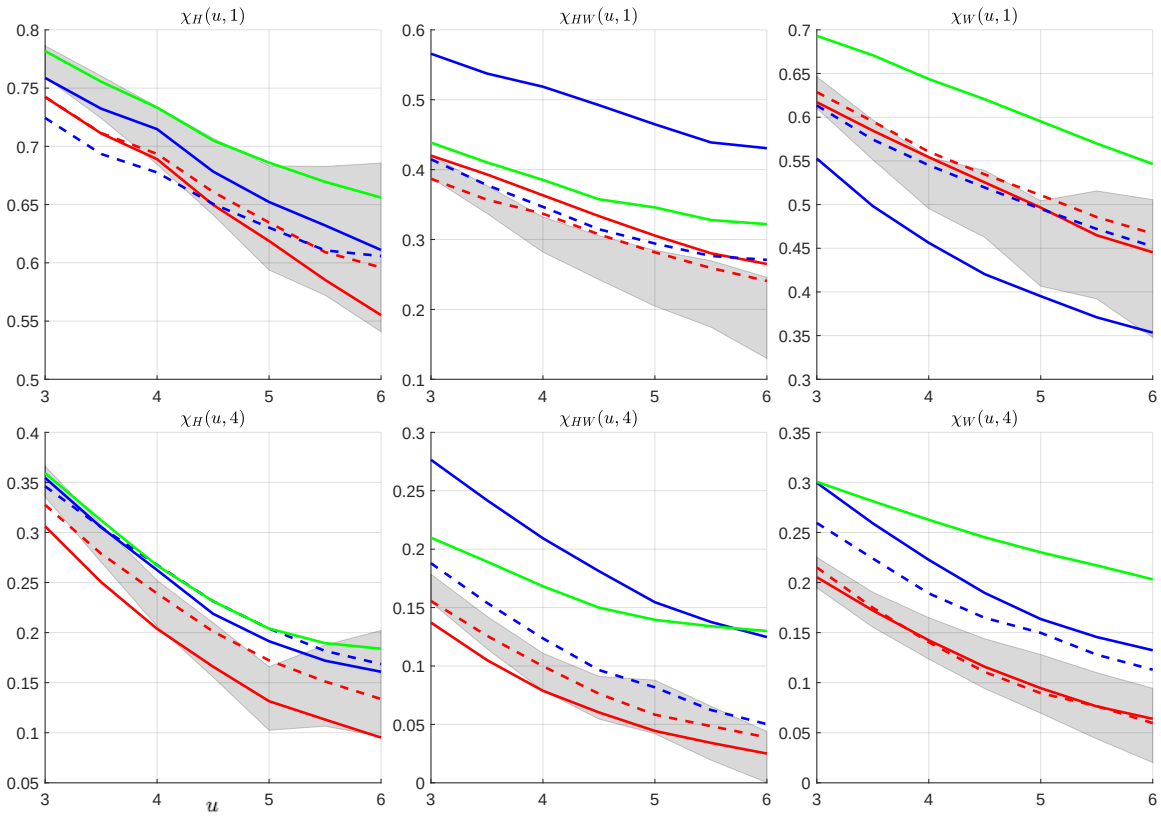

Figure 6: Estimates of measures of extremal dependence across time lags 1 and 4, and variables given by χ_H, χ_{HW} and χ_W (left, middle, and right respectively) for each of the models: EVAR (red), MMEM (blue), HM (green), data (grey). For EVAR and MMEM, we plot these estimates for different model orders $k = 1$ and $k = 4$ with line types: one (solid), four (dotted). Moreover, the grey region depicts the confidence bounds for empirical estimates of these extremal dependence measures from the data.

function) as the mean absolute relative error over these percentiles, i.e.,

$$D(F_M, F_E; p_1, \ldots, p_{20}) = \frac{1}{20} \sum_{j=1}^{20} \left| \frac{F_E^{-1}(p_j) - F_M^{-1}(p_j)}{F_E^{-1}(p_j)} \right|.$$

We remark that in the above definition, we never divide by zero because we only use D to measure the dissimilarity of distributions of positive random variables.

In Figure 7, we show the results for the 50 random partitions of the original sample by plotting the average distance D (with 80% confidence intervals) for each model together with HM for four different structure response variables corresponding to two choices of c and h for each of $R^{\max}$ and R^{sum}. Note that similar studies for other values of c and h for $R^{\max}$ and R^{sum} were examined, and general findings are consistent with those illustrated in Figure 7. For legibility, we omit confidence bands for EVAR_0 since the difference with EVAR is minimal. Model selection now involves choosing the model that yields the smallest average dissimilarity D whilst keeping the model order as low as possible.

We make a number of observations. For the $R^{\max}$ response, EVAR and MMEM clearly outperform HM regardless of model order. However, for the R^{sum} response, high order (e.g., $k = 4, 5, 6$) EVAR and MMEM are necessary to be competitive with HM. We observe also that performance of EVAR and MMEM does not significantly improve or worsen for $k > 4$. This finding is further supported with an unpublished study with Markov model orders of $k \leq 10$. We note that llustrations of excursions in the supplementary material demonstrate that MMEM(1) does not explain the variability of the pre-peak and post-peak periods well.

By looking at the average relative errors in $R^{\max}$ and R^{sum} of our proposed selection of methods, we conclude that a third or fourth order MMEM and a fourth order EVAR are competitive models within their class. Since these models have similar performance, we prefer EVAR(4) because of its simpler two-dimensional residual distribution.

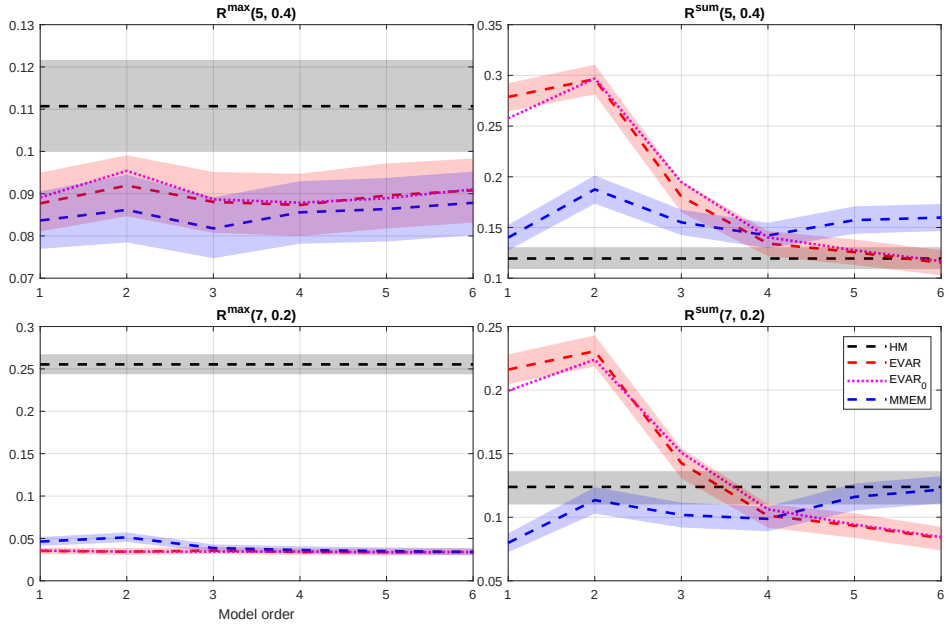

Figure 7: Average mean relative errors of HM, EVAR, EVAR_0 and MMEM (dashed/dotted) and 80% confidence regions (shaded) for estimating the distribution of structure responses using 25% of data for training and 75% of data for testing. For details, see the text.

4 Conclusions and discussion

In this paper, we provide models for extreme excursions of multivariate time-series. Excursions are characterized by a three-stage modelling procedure for the period of the peak, the pre-peak and the post-peak periods. We model the period of the peak using the conditional extremes framework (Heffernan and Tawn, 2004), and for the pre-peak and post-peak periods, we define two classes of time-series models: MMEM, motivated by the Markov extremal model of Winter and Tawn (2017); and EVAR, an extreme-value extension of a vector autoregressive model. We compare these excursion models with a baseline historical matching method, motivated by Feld et al. (2015). We find that the excursion models - for a reasonably informed choice of k, the order of the Markov process - are at least competitive with historical matching and often outperform it in the estimation of the tail of a range of notional structure response variables for a met-ocean application in the northern North Sea.

Statistical modelling of extreme excursions of multivariate time-series is difficult as it requires the estimation of complex model forms. MMEM requires the estimation of the conditional distribution of high-dimensional residual random variables and EVAR is highly parameterized. Model checking for MMEM and EVAR can therefore be challenging. Nevertheless, plots of residuals from model fits on explanatory variables indicate in general that model fits are reasonable. For realistically sized directional samples of significant wave height and wind speed time-series, we found that MMEM(4) and EVAR(4) perform well. Even when the empirical historical matching procedure is competitive, adoption of an excursion model is advantageous because it allows for rigorous uncertainty quantification. We expect that our excursion models are applicable more generally, e.g., for the modelling of higher-dimensional met-ocean time-series and spatial fields.

We model wind speed and significant wave height marginally conditional on directional covariates. In the current work, the marginal transformation to standard Laplace scale does not accommodate seasonal variation. Since only the most extreme excursions are selected for analysis per direction, we are effectively focussing on excursions from the winter period. If the objective of our analysis is a description of the directional evolution of the most extreme excursions with direction, it can be argued (e.g. Mackay et al. 2010, Mackay and Jonathan 2020) that the current approach is acceptable. However, if our objective is to characterise directional evolution as a function of peak direction and season, and the sample data are sufficiently informative, then directional-seasonal marginal models should be preferred (e.g. Jones et al. 2016, Mackay and Jonathan 2020). Moreover, we did not investigate the explicit effect of the directional components on the dependence models. Since we remove the marginal effect of direction before modelling the dependence, we do not expect this covariate to have a strong impact on the dependence. However, it would be very interesting to adapt our models to be able to investigate this further in future research.

Acknowledgement

We thank two reviewers and associate editor for comments on an earlier version of the article. Software for the analysis and illustrative data sets can be found at `github.com/stantendijck/ExtremalExcursions`.

A Reparameterization of EVAR

As opposed to inference for vector autoregressive models, we cannot estimate the EVAR parameters (see Section 2.4) by least squares due to the presence of the $Y_{t,1}^{\mathbf{B}}$ term. Instead, we apply the inference methodology discussed in Section 2.5. Not surprisingly, the parameter estimates $\hat{\Phi}^{(l)}$ for $l = 1, \ldots, k$ are highly intercorrelated because of the linear dependence between the components of $\mathbf{Y}_{t-1}, \ldots, \mathbf{Y}_{t-k}$. Reparameterization to reduce the correlation between parameter estimators is therefore attractive.

To reparameterize the model, we proceed as follows. First, we assume that the conditional extremes model is applicable to $Y_{t-l,j}$ conditional on $Y_{t-k,1}$ for each $l = 0, \ldots, k$ and $j = 1, \ldots, d$ apart from $(l, j) = (k, 1)$,

i.e., there exist parameters $\alpha_{l,j} \in [-1,1]$ and $\beta_{l,j} < 1$ such that

$$\lim_{y\to\infty} \mathbb{P}\left(\frac{Y_{t-l,j} - \alpha_{l,j} y}{y^{\beta_{l,j}}} \leq x \;\middle|\; Y_{t-k,1} = y \right) = H_{l,j}(x),$$

where $H_{l,j}$ is a non-degenerate distribution function. Following the EVAR model (7), we now must have

$$\begin{aligned} Y_{t+k,1} &= \Phi_{1,1}^{(1)} Y_{t+k-1,1} + \cdots + \Phi_{d,1}^{(1)} Y_{t+k-1,d} + \cdots + \Phi_{1,1}^{(k)} Y_{t,1} + \cdots + \Phi_{d,1}^{(k)} Y_{t,d} + Y_{t,1}^{B_1} \varepsilon_{t,1} \\ &= \left(\Phi_{1,1}^{(1)} \alpha_{k-1,1} + \cdots + \Phi_{d,1}^{(1)} \alpha_{k-1,d} + \cdots + \Phi_{1,1}^{(k)} + \cdots + \Phi_{d,1}^{(k)} \alpha_{0,d} \right) Y_{t,1} + o_p(Y_{t,1}) \end{aligned}$$

conditional on $Y_{t,1} > v$ as v tends to infinity. On the other hand, we have $Y_{t+k,1} | (Y_{t,1} > v) = \alpha_{0,1} Y_{t,1} + o_p(Y_{t,1})$. So,

$$\alpha_{0,1} = \Phi_{1,1}^{(1)} \alpha_{k-1,1} + \cdots + \Phi_{d,1}^{(1)} \alpha_{k-1,d} + \cdots + \Phi_{1,1}^{(k)} \cdot 1 + \cdots + \Phi_{d,1}^{(k)} \alpha_{0,d},$$

which explains the collinearity of the estimators. We now propose the following reparameterization $(\mathbf{B}, \tilde{\Phi}^{(1)}, \ldots, \tilde{\Phi}^{(k)})$. For each $1 \leq l \leq d$, we acquire $\tilde{\Phi}_{j,j'}^{(k-l)}$, i.e., the (j,j')th element of $\tilde{\Phi}^{(k-l)}$, inductively with $0 \leq l \leq k-1$, $1 \leq j \leq d$.

$$\Phi_{j,j'}^{(k-l)} = \begin{cases} \hat{\alpha}_{0,j'} + \tilde{\Phi}_{1,j'}^{(k)}, & \text{for } l = 0,\ j = 1, \\ -\tilde{\Phi}_{j-1,j'}^{(k-l)} \cdot \hat{\alpha}_{l,j-1} / \hat{\alpha}_{l,j} + \tilde{\Phi}_{j,j'}^{(k-l)}, & \text{for } l = 0, \ldots, k-1,\ j = 2, \ldots, d, \text{ conditional on } \tilde{\Phi}_{1,j'}^{(k-l)}, \\ -\tilde{\Phi}_{d,j'}^{(k-l+1)} \cdot \hat{\alpha}_{l-1,d} / \hat{\alpha}_{l,1} + \tilde{\Phi}_{1,j'}^{(k-l)}, & \text{for } l = 1, \ldots, k-1,\ j = 1 \text{ conditional on } \tilde{\Phi}_{d,j'}^{(k-l+1)}. \end{cases}$$

where $\hat{\alpha}_{l,j}$ is the maximum likelihood estimate for $\alpha_{l,j}$. Under this reparametrization, estimators of $\tilde{\Phi}_{j,j'}^{(l)}$ are less correlated, which we demonstrated in unreported experiments comparing the dependence of the original and the reparameterized parameters using adaptive MCMC methodology (Roberts and Rosenthal, 2009).

References

Bauwens, L., Laurent, S., Rombouts, J.V., 2006. Multivariate GARCH models: a survey. Journal of Applied Econometrics 21, 79–109.

Bortot, P., Coles, S., 2003. Extremes of Markov chains with tail switching potential. Journal of the Royal Statistical Society: Series B (Statistical Methodology) 65, 851–867.

Bortot, P., Tawn, J.A., 1998. Models for the extremes of Markov chains. Biometrika 85, 851–867.

Chavez-Demoulin, V., Davison, A.C., 2005. Generalized additive modelling of sample extremes. Journal of the Royal Statistical Society: Series C (Applied Statistics) 54, 207–222.

Coles, S.G., Tawn, J.A., 1994. Statistical methods for multivariate extremes: an application to structural design (with discussion). Journal of the Royal Statistical Society: Series C (Applied Statistics) 43, 1–31.

Davison, A.C., Smith, R.L., 1990. Models for exceedances over high thresholds (with discussion). Journal of the Royal Statistical Society: Series B (Methodological) 52, 393–425.

Eastoe, E.F., Tawn, J.A., 2012. Modelling the distribution of the cluster maxima of exceedances of sub-asymptotic thresholds. Biometrika 99, 43–55.

Feld, G., Randell, D., Wu, Y., Ewans, K., Jonathan, P., 2015. Estimation of storm peak and intrastorm directional–seasonal design conditions in the North Sea. Journal of Offshore Mechanics and Arctic Engineering 137.

Gandy, A., Jana, K., Veraart, A.E., 2022. Scoring predictions at extreme quantiles. AStA Advances in Statistical Analysis 106, 527–544.

Heffernan, J.E., Tawn, J.A., 2004. A conditional approach for multivariate extreme values (with discussion). Journal of the Royal Statistical Society: Series B (Methodology) 66, 497–546.

Hilal, S., Poon, S.H., Tawn, J.A., 2011. Hedging the black swan: Conditional heteroskedasticity and tail dependence in S&P500 and VIX. Journal of Banking & Finance 35, 2374–2387.

Janßen, A., Segers, J., 2014. Markov tail chains. Journal of Applied Probability 51, 1133–1153.

Joe, H., 1997. Multivariate Models and Multivariate Dependence Concepts. CRC Press.

Jones, M., Randell, D., Ewans, K., Jonathan, P., 2016. Statistics of extreme ocean environments: non-stationary inference for directionality and other covariate effects 119, 30–46.

Keef, C., Papastathopoulos, I., Tawn, J.A., 2013. Estimation of the conditional distribution of a multivariate variable given that one of its components is large: Additional constraints for the Heffernan and Tawn model. Journal of Multivariate Analysis 115, 396–404.

Leadbetter, M.R., Lindgren, G., Rootzén, H., 1983. Extremes and Related Properties of Random Sequences and Processes. New York: Springer-Verlag.

Ledford, A.W., Tawn, J.A., 2003. Diagnostics for dependence within time series extremes. Journal of the Royal Statistical Society: Series B (Statistical Methodology) 65, 521–543.

Lugrin, T., Davison, A.C., Tawn, J.A., 2016. Bayesian uncertainty management in temporal dependence of extremes. Extremes 19, 491–515.

Ma, L., Swan, C., 2020. The effective prediction of wave-in-deck loads. Journal of Fluids and Structures 95, 102987.

Mackay, E., Jonathan, P., 2020. Assessment of return value estimates from stationary and non-stationary extreme value models 207, 107406.

Mackay, E.B.L., Challenor, P.G., Bahaj, A.S., 2010. On the use of discrete seasonal and directional models for the estimation of extreme wave conditions 37, 425–442.

Morison, J., Johnson, J., Schaaf, S., 1950. The force exerted by surface waves on piles. Journal of Petroleum Technology 2, 149–154.

Papastathopoulos, I., Casey, A., Tawn, J.A., 2023. Hidden tail chains and recurrence equations for dependence parameters associated with extremes of higher-order Markov chains. Submitted .

Papastathopoulos, I., Strokorb, K., Tawn, J.A., Butler, A., 2017. Extreme events of Markov chains. Advances in Applied Probability 49, 134–161.

Perfekt, R., 1997. Extreme value theory for a class of Markov chains with values in $\mathbb{R}^d$. Advances in Applied Probability 29, 138–164.

Randell, D., Feld, G., Ewans, K., Jonathan, P., 2015. Distributions of return values for ocean wave characteristics in the South China Sea using directional–seasonal extreme value analysis. Environmetrics 26, 442–450.

Reistad, M., Breivik, O., Haakenstad, H., Aarnes, O.J., Furevik, B.R., 2009. A high-resolution hindcast of wind and waves for the North Sea, the Norwegian Sea and the Barents Sea. Norwegian Meteorological Institute .

Roberts, G.O., Rosenthal, J.S., 2009. Examples of adaptive MCMC. Journal of Computational and Graphical Statistics 18, 349–367.

Rootzén, H., 1988. Maxima and exceedances of stationary Markov chains. Advances in Applied Probability 20, 371–390.

Ross, E., Astrup, O.C., Bitner-Gregersen, E., Bunn, N., Feld, G., Gouldby, B., Huseby, A., Liu, Y., Randell, D., Vanem, E., Jonathan, P., 2020. On environmental contours for marine and coastal design. Ocean Engineering 195, 106194.

Shooter, R., Ross, E., Ribal, A., Young, I.R., Jonathan, P., 2022. Multivariate spatial conditional extremes for extreme ocean environments. Ocean Engineering 247, 110647.

Simpson, E.S., Wadsworth, J.L., 2021. Conditional modelling of spatio-temporal extremes for Red Sea surface temperatures. Spatial Statistics 41, 100482.

Smith, R.L., 1992. The extremal index for a Markov chain. Journal of Applied Probability 29, 37–45.

Smith, R.L., Tawn, J.A., Coles, S.G., 1997. Markov chain models for threshold exceedances. Biometrika 84, 249–268.

Tendijck, S., Ross, E., Randell, D., Jonathan, P., 2019. A model for the directional evolution of severe ocean storms. Environmetrics 30, e2541.

Tiao, G.C., Box, G.E., 1981. Modeling multiple time series with applications. Journal of the American Statistical Association 76, 802–816.

Tiao, G.C., Tsay, R.S., 1989. Model specification in multivariate time series. Journal of the Royal Statistical Society: Series B (Methodological) 51, 157–195.

Towe, R.P., Tawn, J.A., Lamb, R., Sherlock, C.G., 2019. Model-based inference of conditional extreme value distributions with hydrological applications. Environmetrics 30, e2575.

Winter, H.C., Tawn, J.A., 2016. Modelling heatwaves in central France: a case-study in extremal dependence. Journal of the Royal Statistical Society: Series C (Applied Statistics) 65, 345–365.

Winter, H.C., Tawn, J.A., 2017. kth-order Markov extremal models for assessing heatwave risks. Extremes 20, 393–415.

Yun, S., 2000. The distributions of cluster functionals of extreme events in a dth-order Markov chain. Journal of Applied Probability 37, 29–44.

Supplementary Information to "Temporal evolution of the extreme excursions of multivariate kth order Markov processes with application to oceanographic data"

Stan Tendijck[1], Philip Jonathan[1,2], David Randell[3], and Jonathan Tawn[1]

[1]Department of Mathematics and Statistics, Lancaster University LA1 4YW, United Kingdom
[2]Shell Research Limited, London SE1 7NA, United Kingdom
[3]Shell Global Solutions International B.V., 1031 HW Amsterdam, Netherlands

October 26, 2023

The supplementary information consists of a series of figures following the format of Figure 5 of the main text, for different model choices.

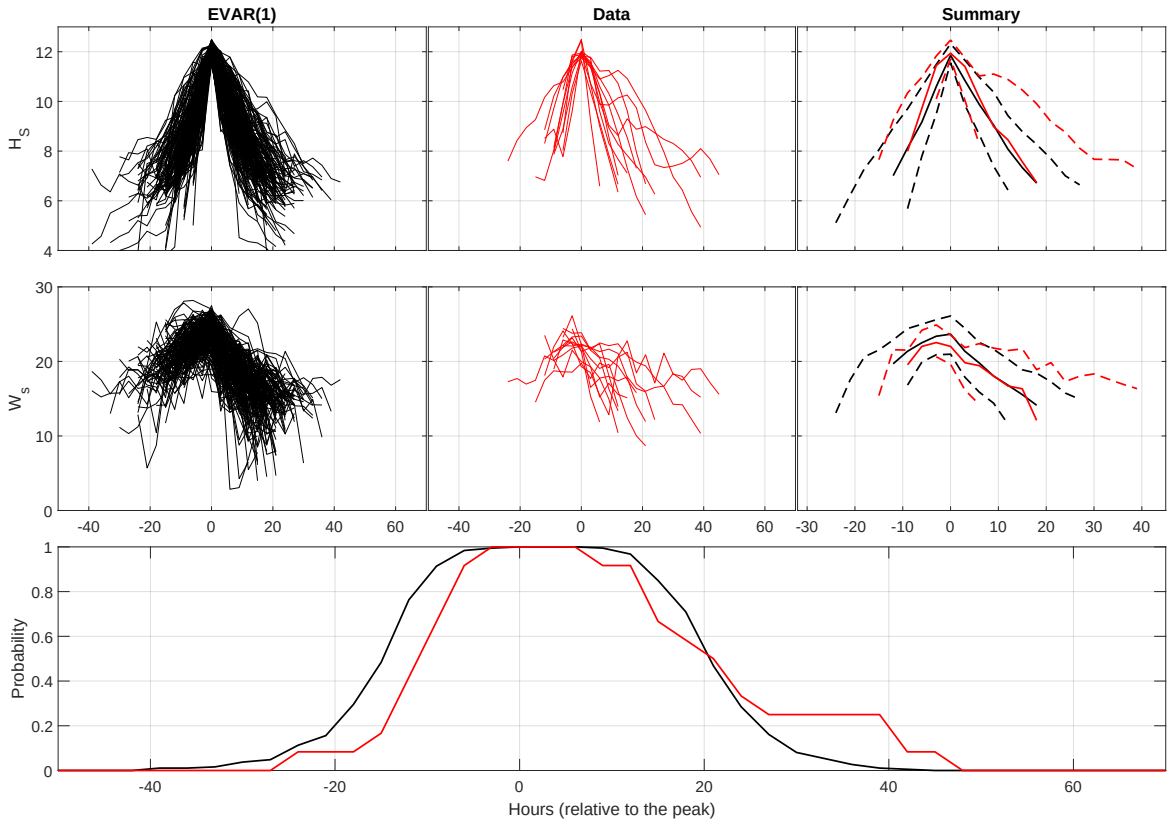

Figure 1: EVAR(1)

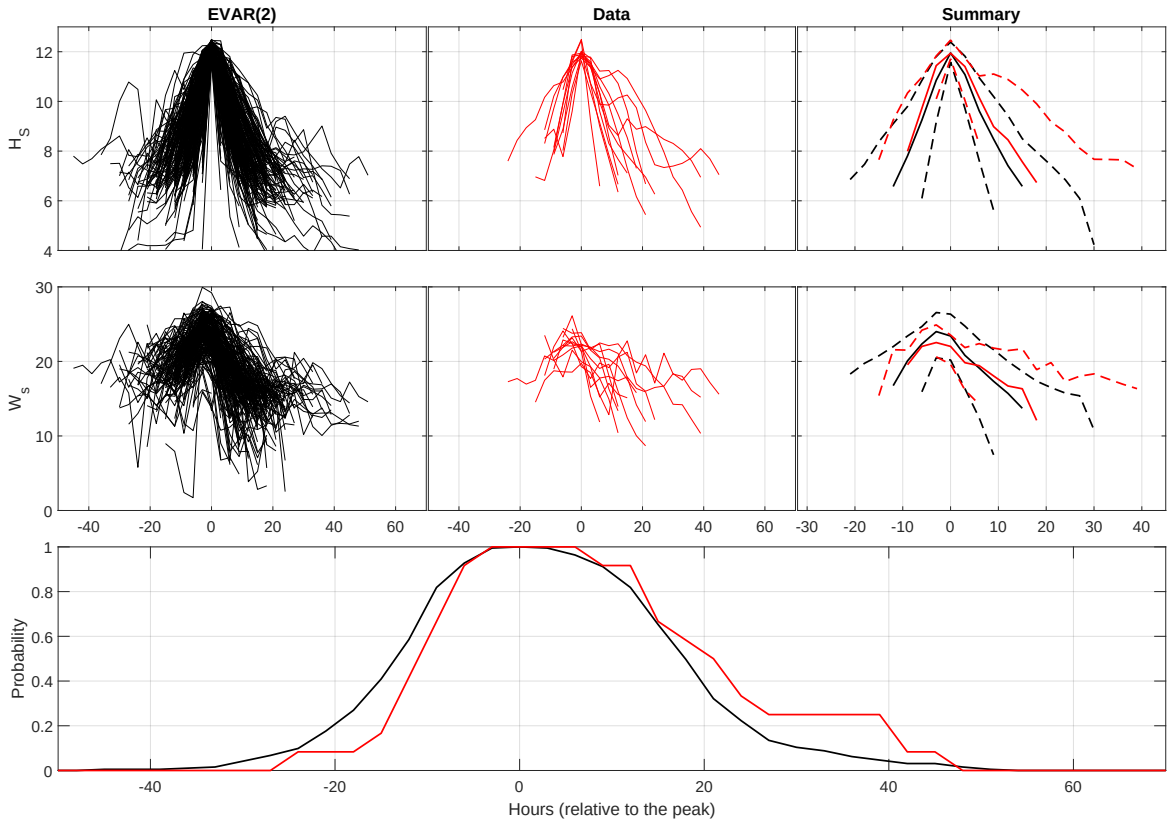

Figure 2: EVAR(2)

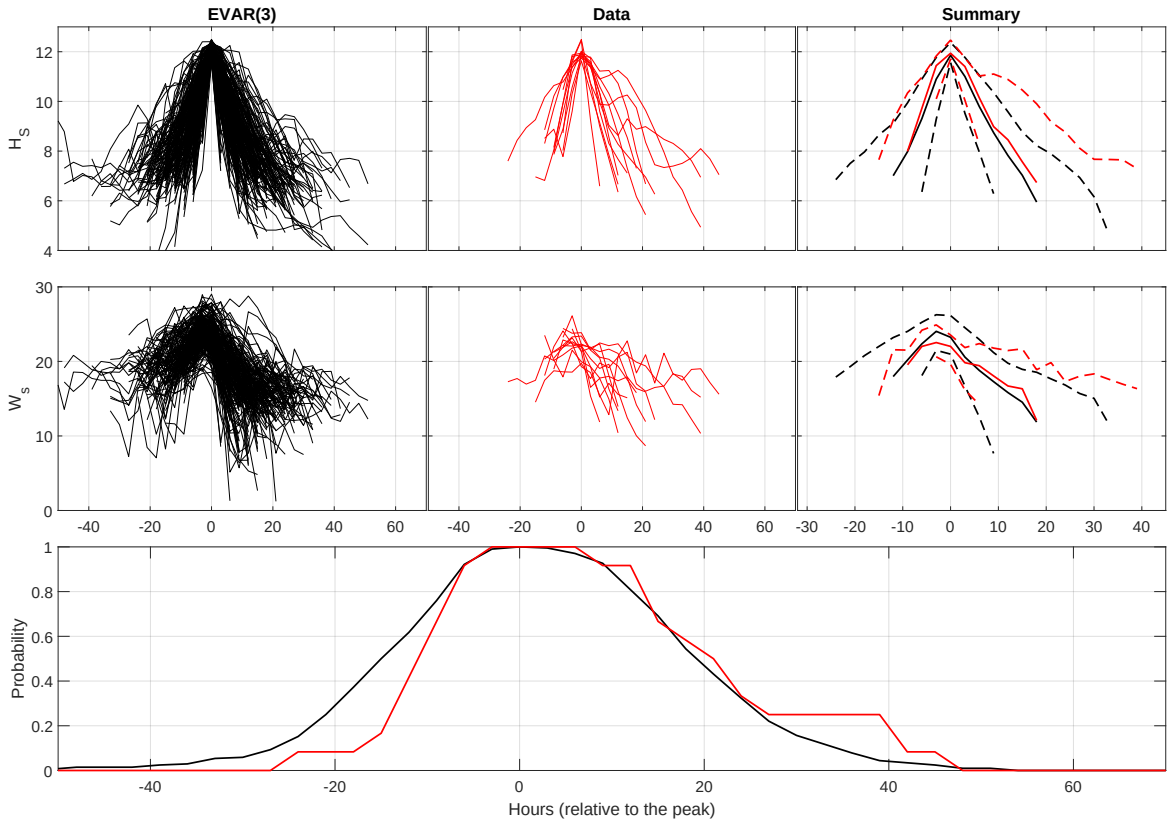

Figure 3: EVAR(3)

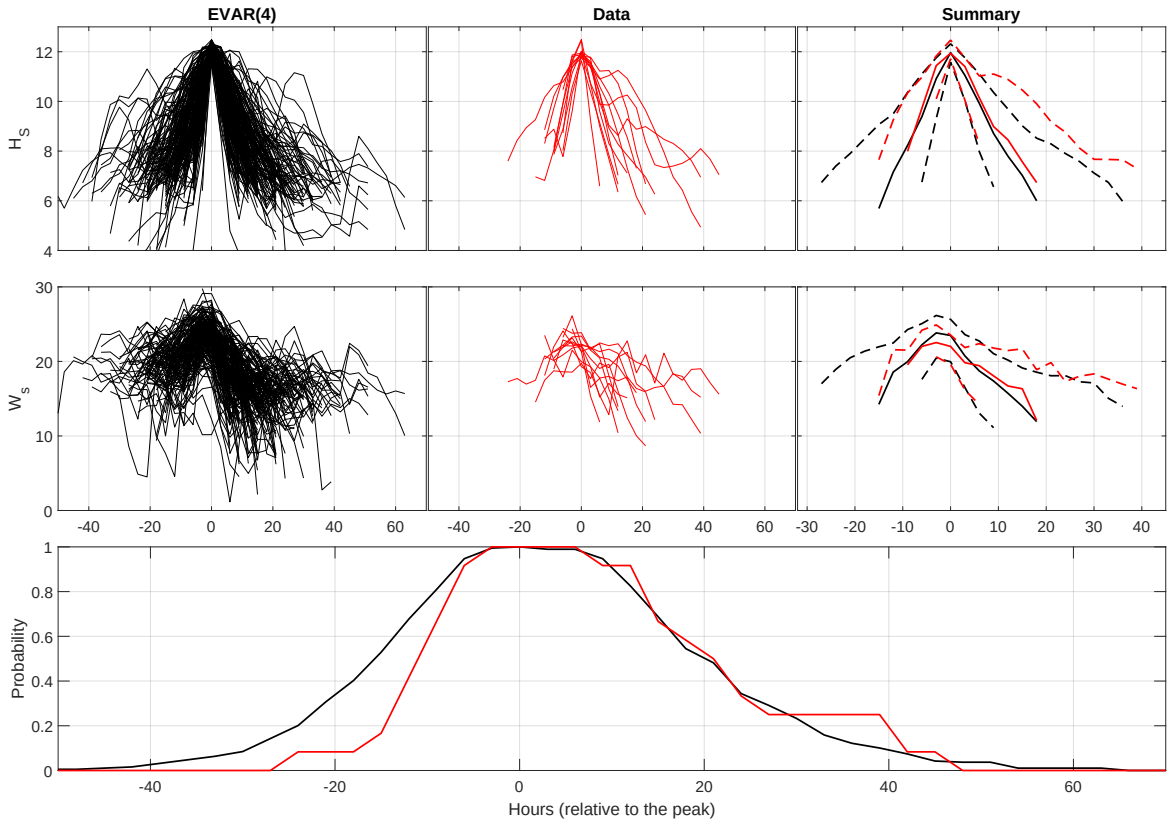

Figure 4: EVAR(4)

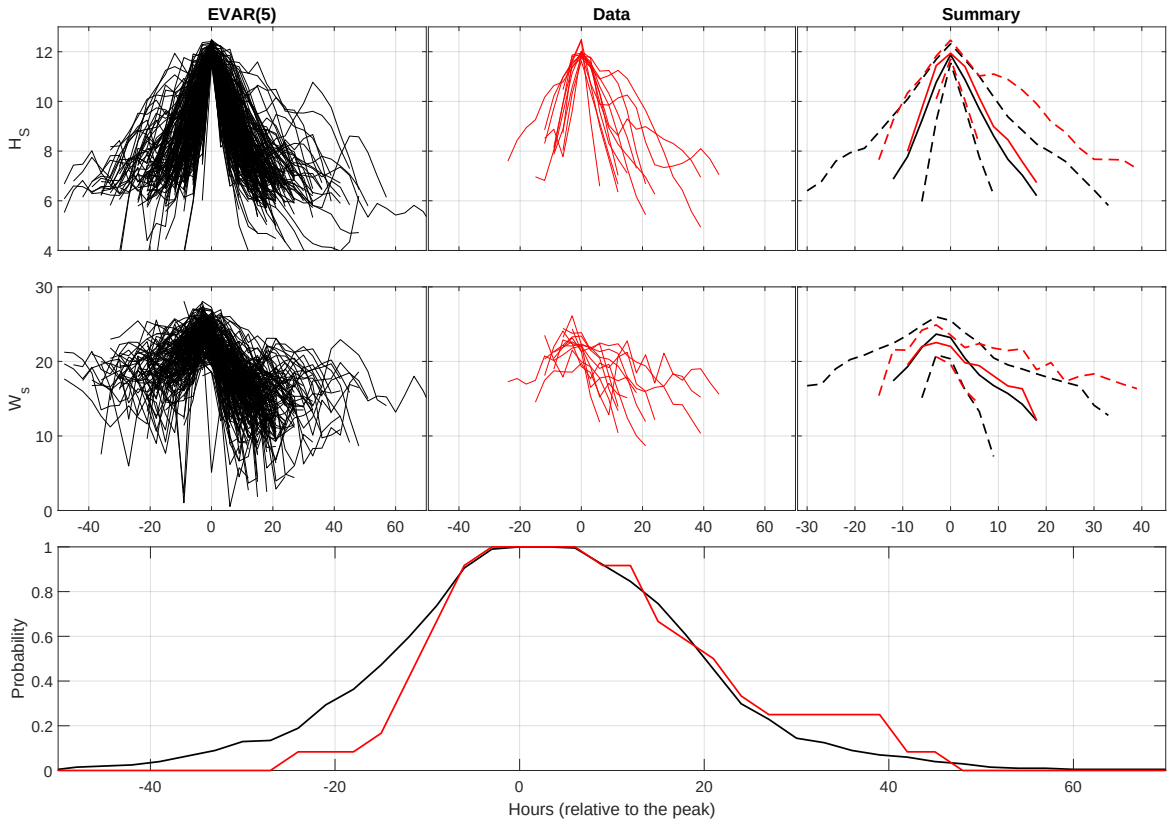

Figure 5: EVAR(5)

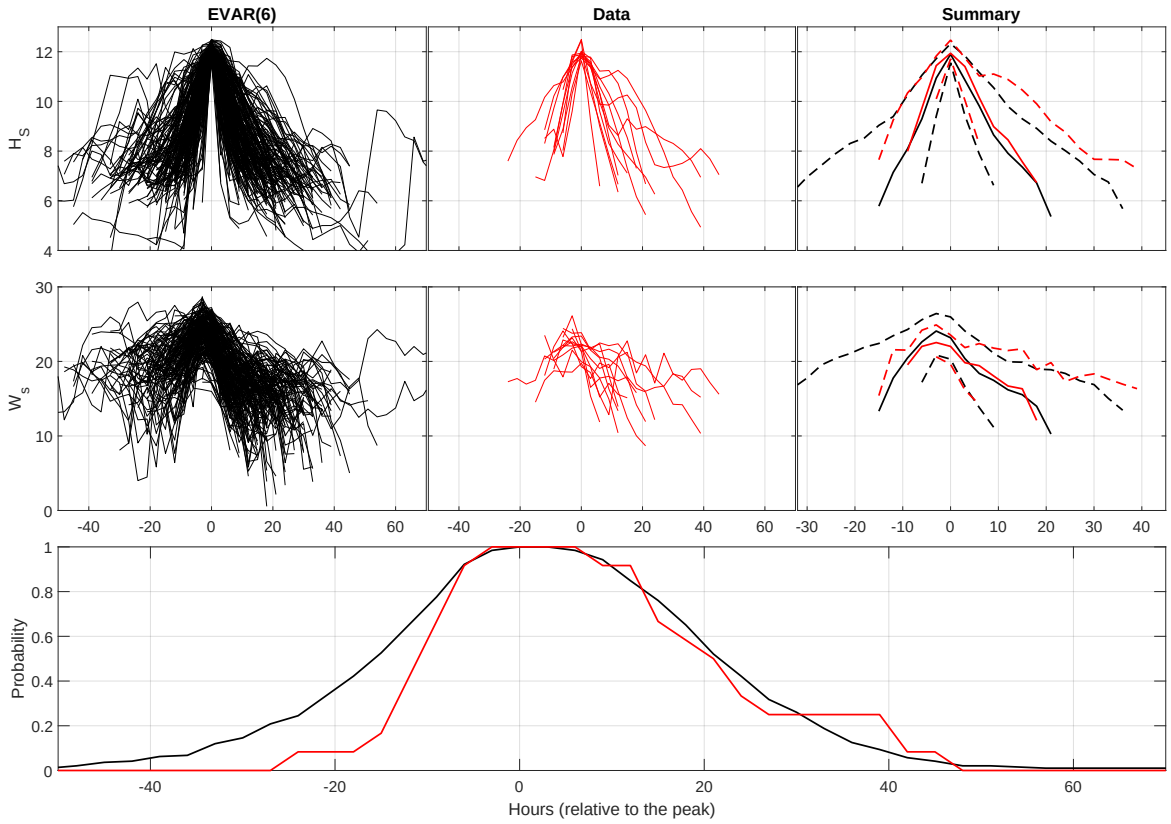

Figure 6: EVAR(6)

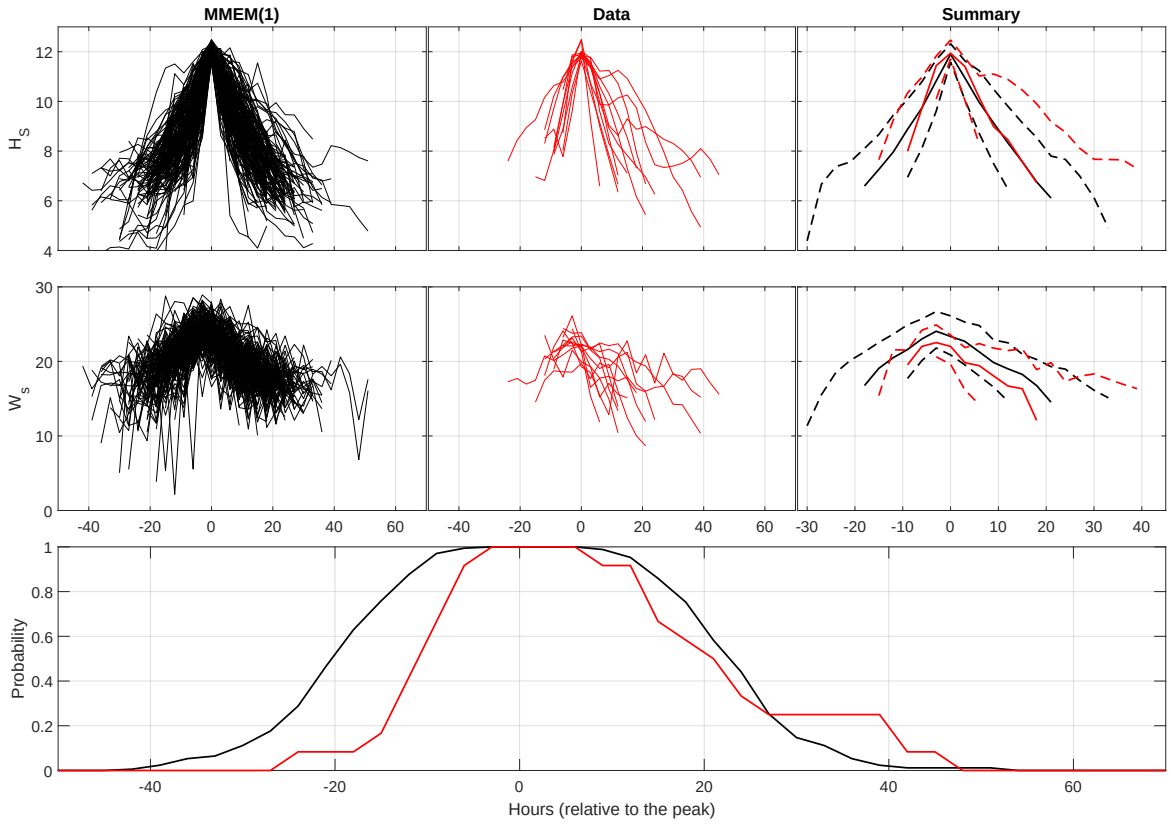

Figure 7: MMEM(1)

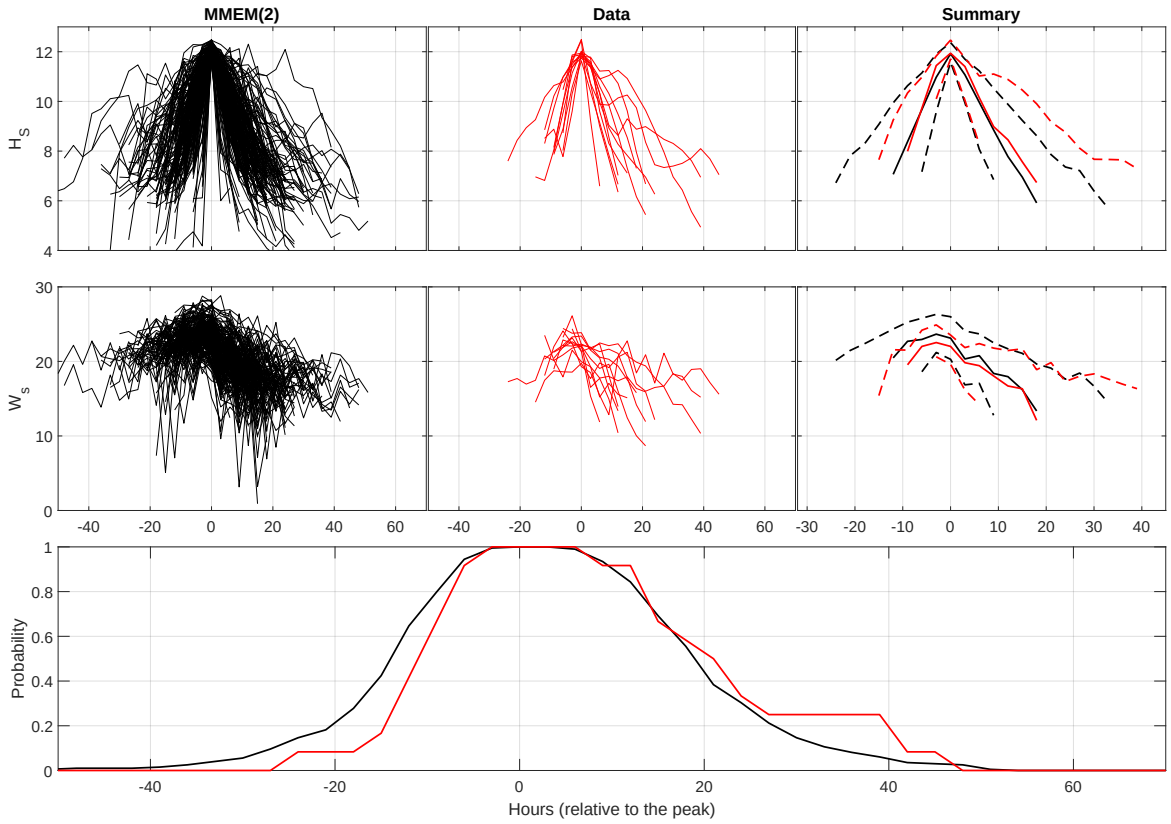

Figure 8: MMEM(2)

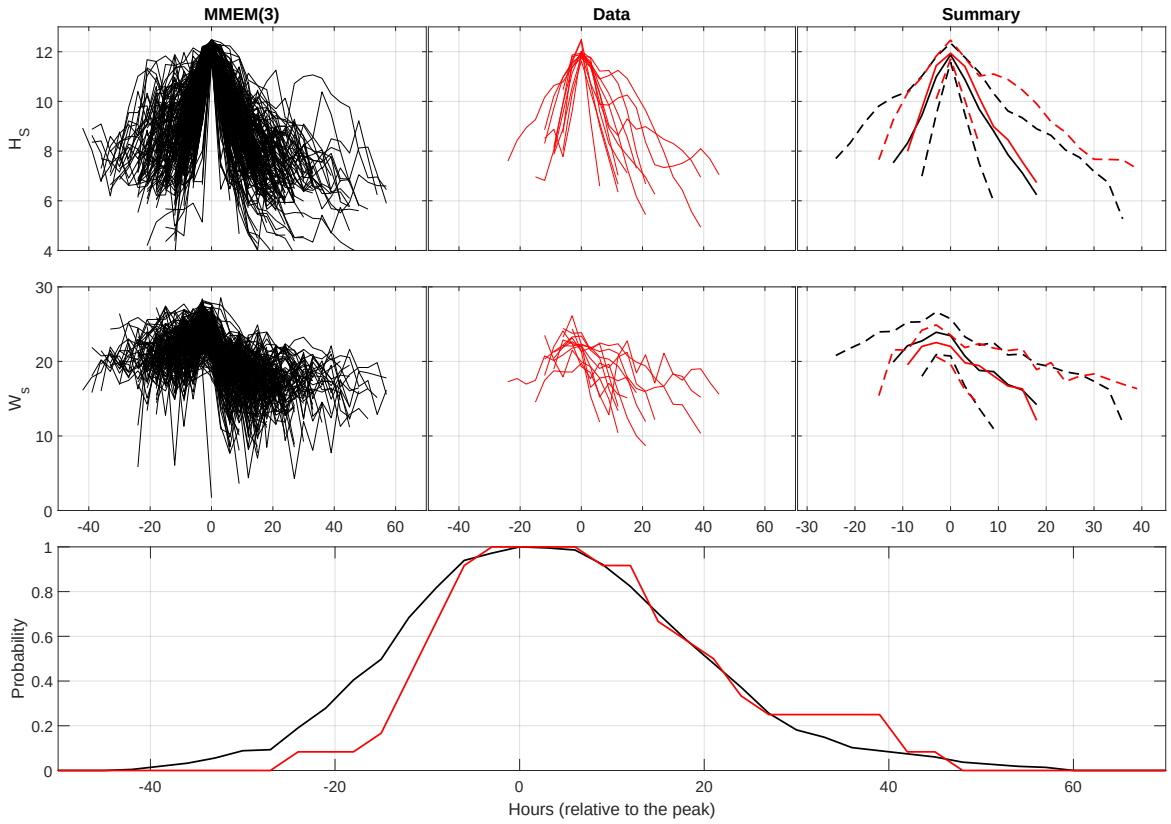

Figure 9: MMEM(3)

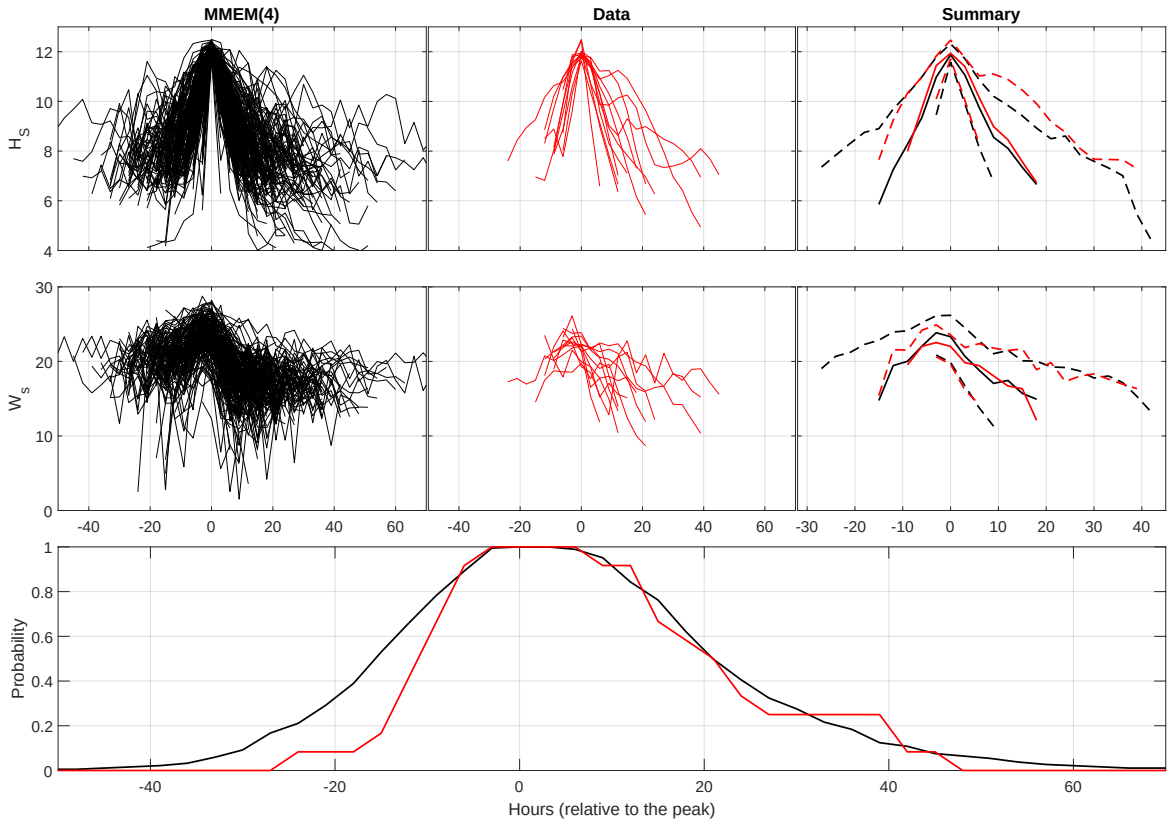

Figure 10: MMEM(4)

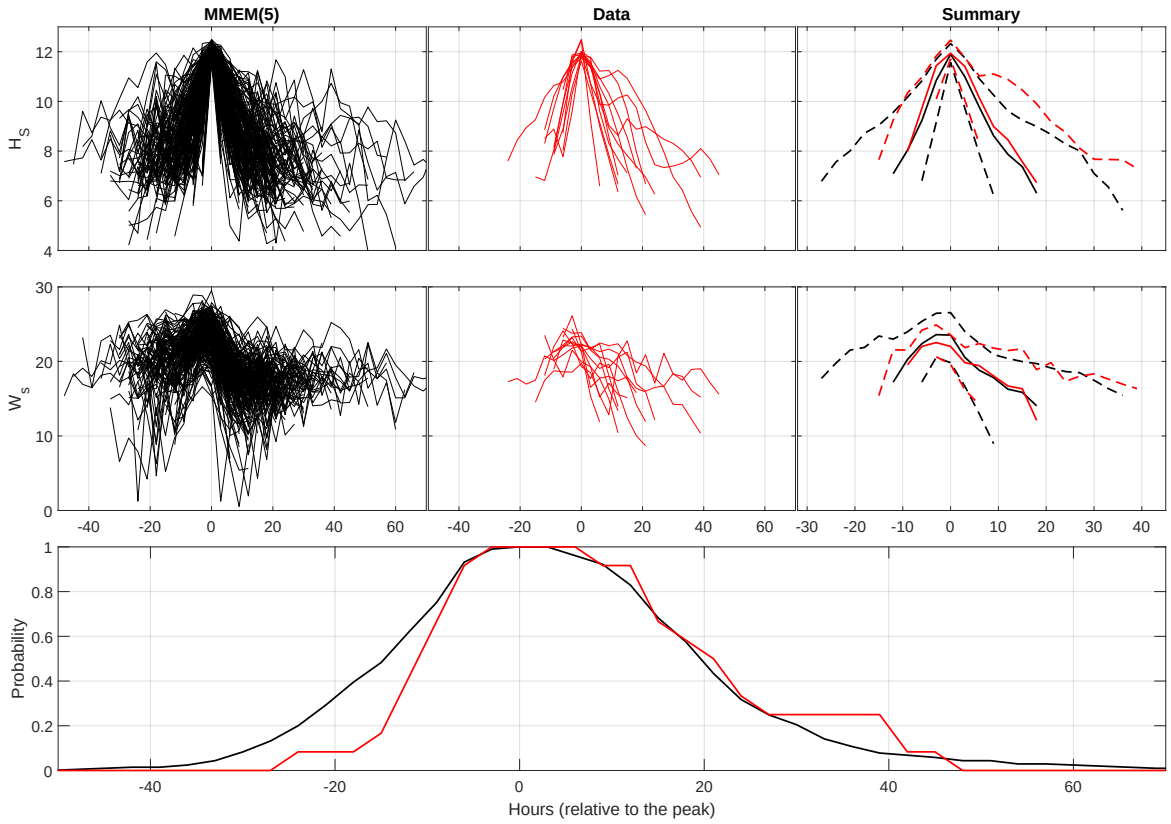

Figure 11: MMEM(5)

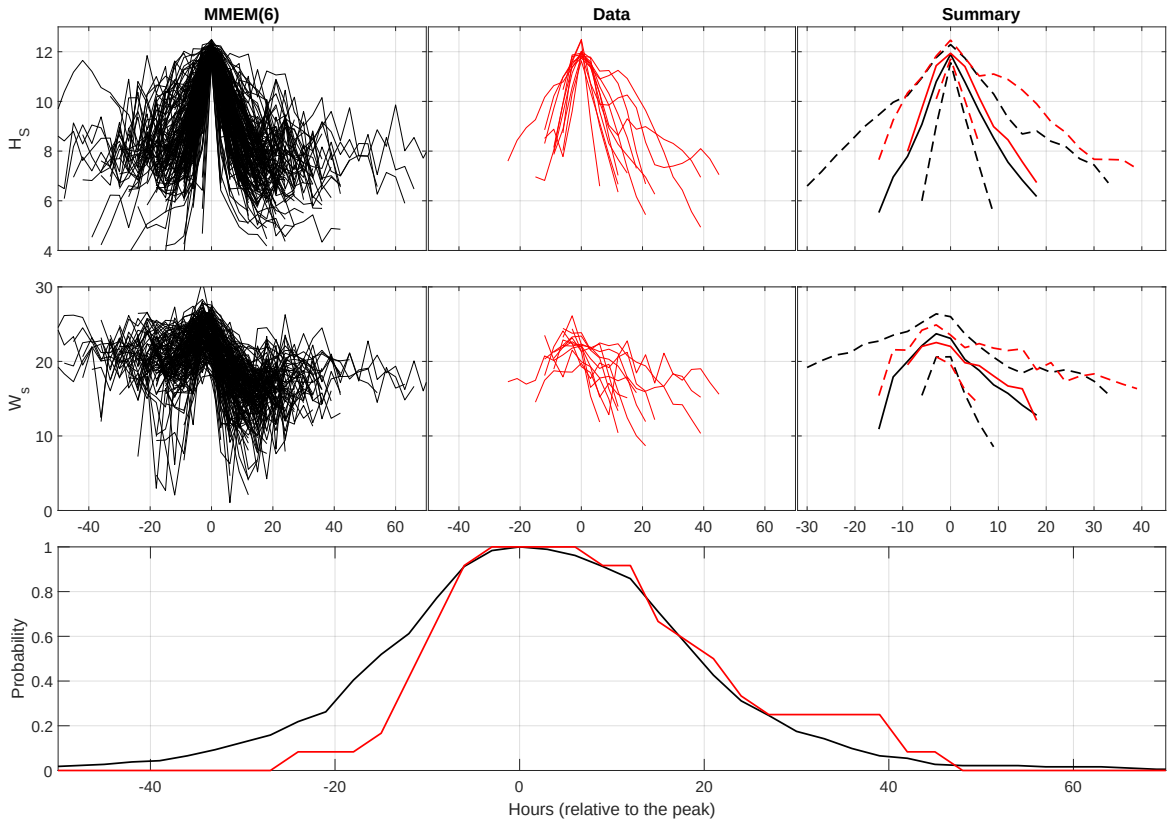

Figure 12: MMEM(6)

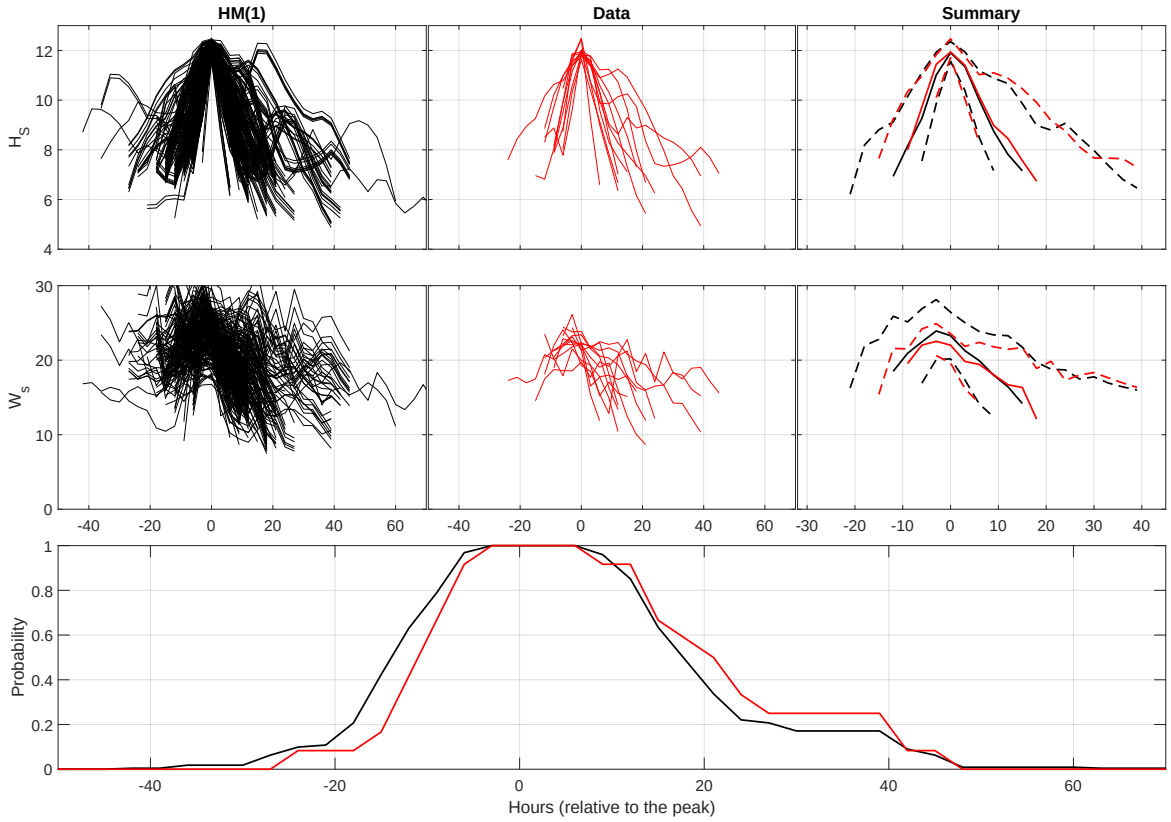
HM(1)
Data
Summary
H_S
W_s
Probability
Hours (relative to the peak)

Figure 13: HM